been determined at resolutions of 3.4 Å, 3.2 Å, and 3.2 Å, respectively. In this study, to understand the structural basis on HEV, we solved the crystal structure of HEV-LP derived from a genotype 3 strain at 3.5-Å resolution and found differences in the folding of the capsid protein among these viruses. On the other hand, we found several structural similarities of shell formation. In particular, it was revealed that aromatic amino acids (Tyr-288 in the case of HEV-LP) at the 5-fold axis play a crucial role in the hydrophobic interaction required for particle formation and are well conserved among these viruses. Furthermore, mutational analyses depicted the putative cellular receptor-binding regions and epitopes for neutralizing of binding (NOB) antibodies on the 3D structure of HEV-LP. The availability of the 3D structure of HEV-LP at high resolution will provide valuable information not only for analyses of the entry and assembly of HEV, but also for the development of a vaccine for hepatitis E.

Results

Preparation of HEV-LP of a Genotype 3. Upon infection with a recombinant baculovirus possessing a genome of the truncated capsid protein (amino acids 112–608) from a genotype 3 strain under the control of polyhedrin promoter, a large amount of HEV-LP was secreted into the culture supernatant as described in the case of HEV-LP of genotype 1 strain (26–28). The purified HEV-LP of genotype 3 was used for further structural and biological analyses.

Overall Structure of HEV-LP. The crystal structure of HEV-LP derived from the genotype 3 strain was determined at 3.5-Å resolution by the molecular replacement method by using a cryoEM map of HEV-LP derived from the genotype 1 strain (27, 28) as an initial phasing model (Fig. 1*A*). As shown in the previous papers (27, 28), HEV-LP shows a $T = 1$ icosahedral symmetry with an external diameter of 270 Å. This particle is composed of 60 subunits of the truncated capsid proteins, forming the icosahedral 2-, 3-, and 5-fold axes. It has 30 protrusions at the 2-fold axis of the surface with large depressions at the 3- and 5-fold axes.

Structure of the HEV Capsid Protein. The truncated HEV capsid protein has 3 definite domains designated as S (shell), M (middle), and P (protruding) composed of the amino acid residues 129–319, 320–455, and 456–606, respectively (Fig. 1*B*). Because the N- and C-terminally truncated capsid proteins were used for the characterization, the typical signal sequence (amino acids 1–22) and following arginine-rich domain (amino acids 23–111) and the C-terminal domain removed by cleavage in insect cells (amino acids 609–660) were not determined in this study. Additionally, the amino acid residues 112–128, 486–487, 555–560, and 607–608 were disordered in this study. The S domain, which forms an internal scaffold structure of the particle, folds into a classical anti-parallel jelly roll-like β-sandwich structure with 8 β-strands (designated as B to I) and 4 short α-helices that are conserved among many viral capsids (Fig. 1*B* and Fig. S1) (29–33). The M domain, which is one of the characteristic domains, has a twisted anti-parallel β-barrel structure composed of 6 β-strands and 4 short α-helices. This domain is tightly associated with the S domain and located on the surface around the icosahedral 3-fold axis (Fig. 1*A* and *B*). The M and P domains are linked with a long proline-rich hinge (amino acids 445–467). Previous studies on the structures of rNV (29) and SMSV (30) revealed that the P domains of the viruses are composed of 2 subdomains, P1 and P2, and the P2 subdomain is located as a large protrusion of the P1 subdomain (Fig. S1). In contrast, the P domain of HEV-LP is composed of a single individual domain forming a twisted anti-parallel β-sheets structure (Fig. 1*B* and Fig. S1), demonstrating that the capsid protein

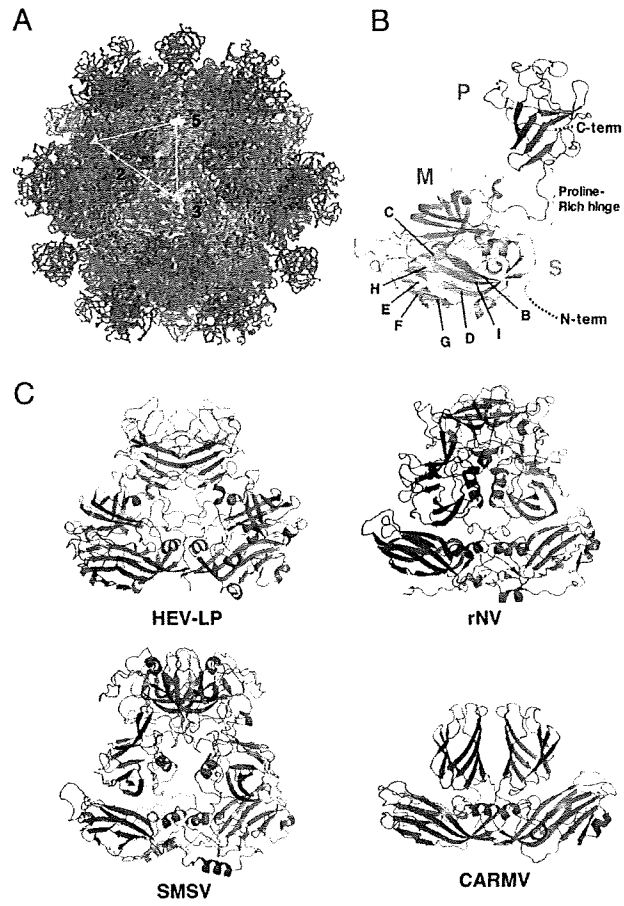

Fig. 1. Crystal structure of HEV-LP and comparison of capsid protein dimers of HEV-LP, rNV, SMSV, and CARMV. The S, M, and P domains of the HEV capsid protein are indicated by pink, green, and blue, respectively. (*A*) HEV-LP is composed of sixty capsid subunits forming icosahedral 2-, 3-, and 5-fold axes and indicating a $T = 1$ symmetry. (*B*) The ribbon diagram of a capsid subunit of HEV-LP (PDB accession code: 2ZTN) shows P, M, and S domains at the top, middle, and bottom, respectively. The disordered regions are shown with dashed lines. The S domain shows a jerry roll-like β-barrel structure conserved in some viruses. The conserved anti-parallel β-strands are indicated (B to I). (*C*) The ribbon diagrams of crystal structures of capsid protein dimers of HEV-LP and those of rNV (PDB accession code 1IHM), SMSV (PDB accession code 2GH8), and CARMV (PDB accession code 1OPO) are indicated. Each capsid protein monomer is colored in red and blue.

of HEV-LP has a significantly different fold from those of caliciviruses, except for the S domain. Although we have no evidence of glycosylation of HEV-LP prepared in insect cells, the HEV capsid protein has 3 potential *N*-glycosylation sites, Asn-137-Leu-Ser, Asn-310-Leu-Thr and Asn-562-Thr-Thr (19). In the dimer structure, the former 2 sites are mapped on the horizontal surface of the S domain, as shown in Fig. S2*A*. However, Asn-137 and Asn-310 are located in the interfaces of the pentamer and trimer structures, respectively (Fig. S2*B* and *C*), suggesting that, if it occurs at all, *N*-glycosylation in these sites may inhibit assembly of HEV-LP. Indeed, Graff et al. (18) reported that HEV carrying mutations in Asn-137 or Asn-310 to Glu lost infectivity to cells or rhesus macaques due to a defect in the virion assembly. On the other hand, Asn-562 is mapped in the central region in the top of the P dimer and exposed in the surface of HEV-LP.

The Dimer Structure at the 2-Fold Axis. It is noteworthy that the HEV-LP dimer at the icosahedral 2-fold axis shows a crossing

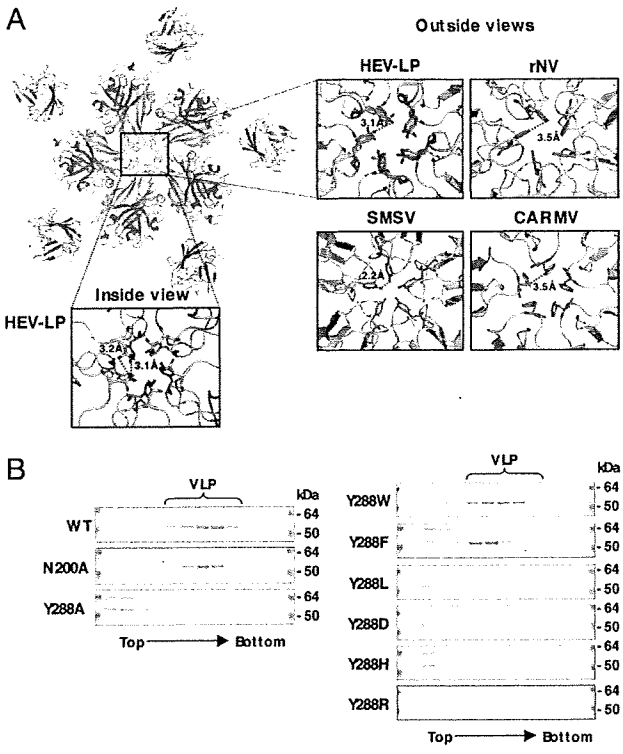

Fig. 2. Interaction of capsid protein subunits of HEV-LP around the 5-fold axis. (*A*) The pentamer of the capsid protein of HEV-LP. The close-up surface diagram of the 5-fold axis showed from outside and inside of HEV-LP. Amino acid residues Asn-200 and Tyr-288 are shown in yellow and green, respectively. The close-up surface diagram of the 5-fold axis showed from outside of rNV, SMSV, and CARMV. The aromatic amino acids Phe-118 of rNV, Tyr-330 of SMSV, and Phe-145 of CARMV are indicated in green. The deduced interacting atoms are connected with dashed lines, and the distances are indicated. (*B*) Sucrose density fractionation assay using the wild-type or mutant capsid proteins (53 kDa) in which the amino acids composing the 5-fold axis were substituted. The capsid protein composing HEV-LP was found in the 5–9th fractions from the top, while that which failed to form particles was found in the top fractions. The molecular mass of approximately 64 kDa was a non-specific protein.

topology of the P versus M and S domains, while that of the other viruses with protrusions at the 2-fold axis, containing rNV, SMSV, and CARMV, exhibits a parallel topology of each domain (Fig. 1*C*). The flexibility of the long proline-rich hinge region between the M and P domains allows this unique topology of HEV-LP. The P domain of HEV-LP interacts with not only the P domain but also the M domain of the counterpart to stabilize the dimer structure. Despite these topological differences, the overall structure of the protrusion dimeric structure at the 2-fold axis is similar to that of rNV and SMSV. The disordered residues 486–487 and 555–560 are located in the apical region of the protrusion, suggesting that this region is flexible to take advantage of the interaction with other molecules.

Five-Fold Axis Packaging. The inter-molecule-interface of the capsid pentamer at the icosahedral 5-fold axis is composed of only S domains, and these interaction regions are narrower than those of the dimer and trimer at the 2-fold and 3-fold axes, respectively (Fig. 2*A*), suggesting that the pentamer formation is a key step of HEV-LP assembly. There are 4 loops between the β-sheets in the S domain, designated as loops B–C (amino acids 139–152), D–E (amino acids 196–206), F–G (amino acids 236–241), and H–I (amino acids 281–296), around the center of the pentamer structure. Among them, the loops B–C and F–G are not in close proximity to the next subunits, suggesting they are not implicated in the inter-molecular interaction. In contrast, loops D–E and H–I do interact with the next subunits. In particular, the side chains of Asn-200 and Tyr-288 in loops D–E and H–I, respectively, interact with those of the next subunits, from which they are separated by a distance of approximately 3.2 Å, filling in the central pore (Fig. 2*A*). These observations led us to hypothesize that these amino acid residues are important for assembly and stability of the particles. To examine this hypothesis, we constructed 2 mutant capsid proteins in which Asn-200 was replaced with alanine (N200A) or Tyr-288 was replaced with alanine (Y288A), and the effect of these mutations on the particle formation was determined by a density-fractionation assay (Fig. 2*B*). Comparative amounts of the mutant proteins to the wild-type capsid were expressed and released into the supernatants of cells infected with the recombinant baculoviruses. N200A but not Y288A formed VLP as the wild-type, indicating that Tyr-288 plays a more crucial role in particle formation than Asn-200. The aromatic amino acids, Phe-118, Tyr-330, and Phe-145, are also found in the icosahedral 5-fold axis of rNV, SMSV, and CARMV, respectively (Fig. 2*A*). To examine the role of the aromatic side chain in Tyr-288 in the particle formation, a series of mutants in which Tyr-288 was replaced with tryptophan, phenylalanine, leucine, asparatic acid, histidine, or arginine (Y288W, Y288F, Y288L, Y288D, Y288H, or Y288R) were generated. All of them were expressed and released into the culture medium, as well as was the wild type. The mutants with aromatic amino acids, Y288W and Y288F, were able to form HEV-LP, whereas other mutants produced no or very few particles (Fig. 2*B*). These results suggest that the aromatic side chain of Tyr-288 plays a crucial role in the HEV-LP formation by shutting off the central pore of the pentamer, and that the aromatic amino acids in the positions corresponding to Tyr-288 of HEV are functionally conserved among the structurally related viruses.

Binding of HEV-LP to Cultured Cells. The early steps of HEV entry remain unclear because of the lack of a robust cell culture system for HEV, despite recent progress in the in vitro propagation of HEV in the cell lines PLC/PRF/5 and A549 (24). HEV-LP was able to bind to several cell lines, including PLC/PRF/5 and A549 cells, but not to mouse myeloma P3 × 63Ag8U.1 (P3U1) cells (Fig. S3), suggesting that a binding assay using HEV-LP is useful to examine the first step of receptor-binding of HEV to the target cells. Among the cell lines examined, the human hepatoma cell line Huh7, exhibited a greater ability to bind to HEV-LP than the cell lines PLC/PRF/5 and A549. Therefore, Huh7 cells were used for the following binding experiments of HEV-LP.

Three-Dimensional Mapping of Epitopes for NOB Antibodies. We examined the ability of the 10 newly produced anti-HEV-LP monoclonal antibodies to inhibit the binding of HEV-LP to Huh7 cells (Fig. 3*A*). Two of the monoclonal antibodies, MAB1323 and MAB272, exhibited NOB of HEV-LP to Huh7 cells and recognized the P domain by immunoblotting using the GST (GST)-fused HEV capsid proteins (Fig. S4). However, further truncation of the C-terminal 28 or N-terminal 24 amino acids from the GST-fused P domain abrogated the binding with the antibodies, indicating that it is difficult to determine the epitopes of the antibodies in more detail using a series of truncated mutants of the P domain. A competitive enzyme-linked immunosorbent assay (ELISA) suggested that MAB1323, MAB272, and MAB161, but not MAB358, which was used as a detector in the binding assay, recognized the same or adjacent epitopes (Fig. S5). The P domains of rNV and feline calicivirus were suggested to be involved in the binding to the receptor molecules (34–36), and we therefore hypothesized that the P

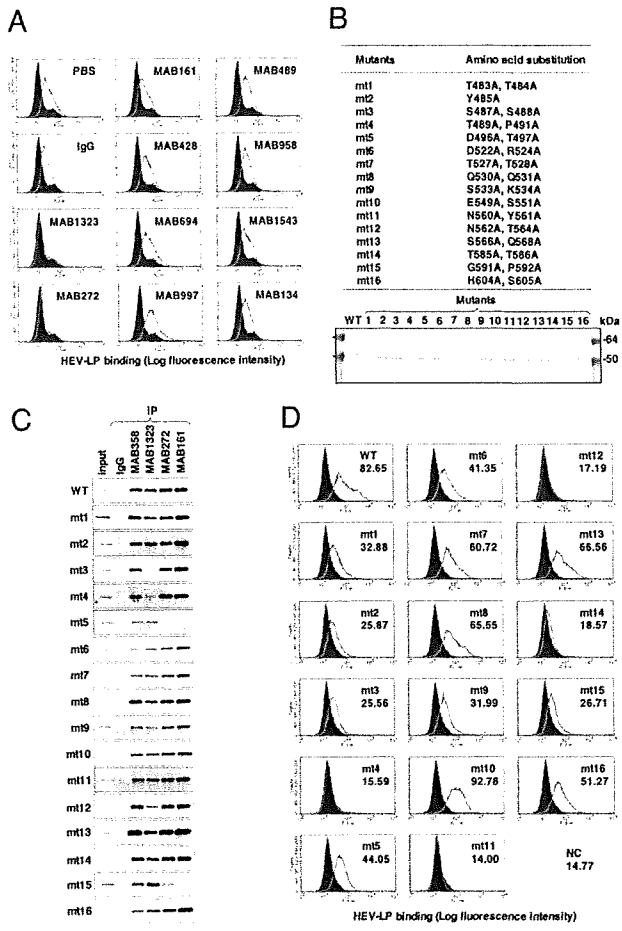

Fig. 3. Characterization of monoclonal antibodies and mutant HEV-LPs. (*A*) Neutralization of binding (NOB) of HEV-LP to Huh7 cells by monoclonal antibodies to HEV-LP. After preincubation of HEV-LP (10 μg/mL) with each of the monoclonal antibodies (20 μg/mL) for 1 h at 37°C, the mixture was inoculated into Huh7 cells and incubated for 1 h at 4°C. HEV-LP (lined area) bound to cells was detected by flow cytometry. The filled area indicates mock-incubated cells. (*B*) Construction of HEV-LP mutants. Sixteen HEV-LP mutants, in which the surface amino acid residues of the P domain were substituted, were constructed. The protein bands of 100 ng each of the purified wild-type and mutant HEV-LPs were visualized by Coomassie brilliant blue staining after SDS/PAGE. (*C*) Reactivities of NOB antibodies with the mutant HEV-LPs. Immunoprecipitation analyses of a series of HEV-LPs by NOB (MAB1323 and MAB272) or non-NOB antibodies (MAB358 and MAB161). Immunoprecipitated HEV-LPs were detected by an anti-HEV capsid rabbit polyclonal antibody. (*D*) Binding capability of the mutant HEV-LPs to Huh7 cells. Wild-type or mutant HEV-LPs (10 μg/mL) were incubated with Huh7 cells for 1 h at 4°C, and then HEV-LP (lined area) bound to cells was detected by flow cytometry. The filled area indicates mock-incubated cells. The MFI is shown in each panel.

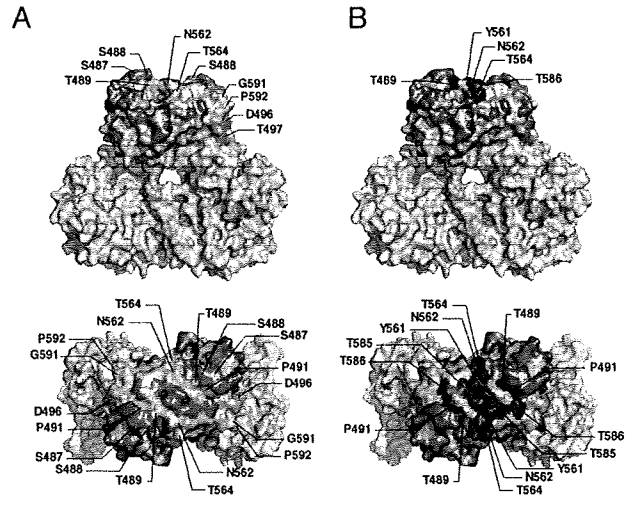

Fig. 4. Amino acid residues involved in the recognition by NOB antibodies and in the binding to Huh7 cells. Surface diagrams of the capsid protein dimer from a lateral (*Upper*) or top (*Lower*) view. (*A*) Amino acids in HEV-LP involved in the complete loss (deep color) or reduction (light color) of reactivity to MAB1323 and MAB272 are shown in orange and green, respectively. (*B*) Amino acids in HEV-LP responsible for binding to Huh7 cells are shown in red. Domains S, M, and P are colored pink, blue and gray, respectively. The substitutions in the P domain of HEV-LP that exhibited no effect on the reactivity with NOB antibodies or the binding to Huh7 cells are shown in dark gray.

domain of HEV-LP might also be involved in the cell binding. To examine this possibility, we prepared 16 HEV-LP mutants in which 1 or 2 amino acid residues at the surface of the P domain were substituted (Fig. 3*B*). The density fractionation assay indicated that all of the mutant proteins formed HEV-LP in the manner of the wild-type capsid protein. MAB358, which recognized an epitope on the M domain (Fig. S4), was capable of precipitating all of the mutants (Fig. 3*C*). MAB1323 exhibited no interaction with mt3 and a weak precipitation of mt4 and mt12. Both MAB272 and MAB161 exhibited no or weak precipitation of mt5 and mt15, whereas MAB272 but not MAB161 exhibited NOB of HEV-LP to Huh7 cells (Fig. 3*A* and *C*). The substituted amino acids of these mutants are illustrated in the 3D structure of the capsid dimer (Fig. 4*A*), and these results suggest that the NOB antibodies MAB1323 and MAB272 recognize the peripheral region of the apical surface (orange) and the horizontal region (green) of the P domain above the M domain at the 3-fold axis, respectively.

Three-Dimensional Mapping of a Region Crucial for Binding to the Target Cells. To determine the region important for binding to the cell surface, the mutant HEV-LPs substituted into the P domain were also used in the assay of binding to Huh7 cells (Fig. 3*D*). The wild-type HEV-LP bound to Huh7 cells with a geographic mean fluorescence intensity (MFI) of 82.65. Among the mutants examined, mt4, mt11, mt12, and mt14 exhibited significantly low MFI values of less than 20. Similar results were obtained using A549 cells (Fig. S6). The amino acid residues required for cell binding were mapped in the central flexible region of the apical surface as shown in Fig. 4*B* (red). This region is partially overlapped with epitopes of MAB1323 (Fig. 4*A*) and other neutralizing antibodies reported by Schofield et al. (16) as shown in Fig. S7. These results suggested that the apical center region of the P domain is involved in the association with not-yet-identified cellular receptor(s).

Discussion

The expression of the truncated HEV capsid protein (amino acids 112–608) in insect cells resulted in assembly of HEV-LP, which retains an antigenicity similar to that of the native HEV particles (26, 37). This particle with a $T = 1$ symmetry has a diameter of 270 Å, which is smaller than the 320-Å diameter of the native virion detected in the fecal specimens of patients (25). It has been reported that the interior cavity of HEV-LP is too small to accommodate a viral RNA of 7.8 kb in length (28) and that the particles show no evidence of nucleotide contents (26, 28). Therefore, native HEV particles are sug-

Table 1. Data collection and processing statistics for HEV-LP

Data collection	
Space group	$P2_12_12_1$
Cell dimensions	
a, *b*, *c*, Å	336.8, 349.4, 359.5
X-ray wavelength, Å	1.0000
Resolution, Å	50–3.55 (3.68–3.55)
R_{merge}*	0.131 (0.498)
$I/\sigma I$	9.8 (3.2)
Completeness, %	99.9 (99.8)
Redundancy	5.6 (5.2)
Refinement	
Resolution range, Å	20–3.56
No. reflections	494,466
R_{work}/R_{free}	30.5/30.9
No. atoms	
Protein	215,400
B factors	
Protein	94.9
rmsd	
Bond length, Å	0.009
Bond angle, °	1.355

Values in square brackets refer to the highest-resolution shell.
*$R_{merge} = \Sigma_{hkl}\Sigma_i|I(hkl)_i - \langle I(hkl)\rangle|/\Sigma_{hkl}I(hkl)$, where $I(hkl)_i$ is the *i*th measurement of the intensity of reflection hkl and $\langle I(hkl)\rangle$ is the mean intensity of reflection *hkl*.

gested to be composed of a larger number and/or a larger size of capsid proteins than HEV-LP. In some cases of plant viruses with a $T = 3$ symmetry, the capsid proteins assembled into particles with a $T = 1$ symmetry by deletion of the N-terminal basic region (38, 39) or amino acid substitutions either in the N-terminal region or in the linker domain between the N-terminal region and S domain (39), suggesting that the N-terminal basic region plays an important role in switching of the transition from $T = 3$ to $T = 1$ symmetry. In addition, expression of the NV capsid protein in insect cells resulted in production of not only $T = 3$ large particles but also small particles thought to have the $T = 1$ symmetry (40). Based on many similarities of the capsid structures and their packaging of structurally related viruses, the native HEV particles are suggested to possess a $T = 3$ surface lattice. The flexibility of the proline-rich hinge linking the M and P domains could allow the capsid protein dimer to switch conformations between the A/B and C/C subunits found in $T = 3$ viruses. Although structure of the native HEV may be slightly different from that of the HEV-LP, the data obtained in this study by using HEV-LP should provide useful information to understand the structure of viral particle, life cycle, and pathogenesis of HEV. The S domain shares the jellyroll fold with some other icosahedral viruses (29–33). It was found that the capsid proteins with substitutions of Tyr-288 positioned at the center of the pentamer structure built in interS domain-interaction failed to assemble into HEV-LP. Alignment analysis of amino acid sequences using data available in GeneBank showed that Tyr-288 is completely conserved within 5 genotypes of HEV. Furthermore, residues corresponding to Tyr-288 of the HEV capsid protein are found in the structures of rNV (Phe-118), SMSV (Tyr-330), and CARMV (Phe-145), although the positions of these aromatic residues are different. Tyr-288 of HEV and Tyr-330 of SMSV located in the H-I loop and Phe-110 of rNV in the D–E loop are exposed at the outside surface of the particles, whereas Phe-145 of CARMV located in the D–E loop is exposed at the interior of the particle. These data suggest that the aromatic side chains of these residues are involved in hydrophobic interactions with those of the next subunits, assuring stable assembly of the particles. During entry into cells, rearrangement of the virion structure is required for release of the genome from the shell. However, the entry and uncoating mechanisms of HEV remain unknown. Because the center of the pentamer is the thinnest region of the particle and takes a channel-like structure (28), this region might also be important for uncoating and release of the viral RNA. It has been proposed that the 5-fold axis of poliovirus is involved in the genomic RNA translocation via conformational change of the virion initiated by binding to the receptor molecules (41, 42).

The first step in viral entry into a target cell is binding to the cellular receptors. The human hepatoma PLC/PRF/5 and lung epithelial A549 cell lines, which are highly susceptible to persistent HEV-infection (24), are likely to express functional HEV receptors on the cell surface. However, HEV-LP had reduced binding to these cells compared to the other cell lines examined. Therefore, the human hepatoma cell line Huh7, which also exhibited a susceptibility to HEV infection (13, 18) and readily bound to HEV-LP, was mainly used in this study. It has been reported that the P domains of noroviruses and the feline calicivirus were involved in the binding to the putative receptors, histo-blood antigens (35, 36) and the feline junctional adhesion molecule (34), respectively. The peptide of the HEV capsid protein (amino acids 368–606), which consists of a part of the M and an entire P domain, was shown to be capable of binding to several cell lines (13), suggesting that the P domain of HEV is also involved in the binding to the cell receptors. Indeed, the mutational analyses in this study indicated that the central flexible region of the top of the P domain of HEV-LP plays a crucial role for binding to Huh7 and A549 cells. This is consistent with a recent study by Graff et al. in which an N562Q mutant of HEV lost infectivity to culture cells and rhesus macaques despite the production of viral particles (18). Interestingly, a possible *N*-glycosylation site, Asn-562-Thr-Thr, is mapped in this region. *N*-glycosylation is an unusual posttranslational modification for nonenveloped viruses, except for rotaviruses (43). The mutant capsid mt12, which has substitutions of Asn-562 and Thr-564 to alanine, exhibited the same migration as the wild-type protein in SDS/PAGE, suggesting that the HEV-LP produced in insect cells was not glycosylated at Asn-562. Lack of *N*-glycosylation in the capsid protein has also been reported in mammalian cells infected with HEV (18), whereas some portion of the capsid protein was glycosylated and transported to the cell surface upon overexpression in mammalian cells (19). *N*-glycosylation of the HEV capsid at Asn-562 may have a negative effect on the receptor-binding, whereas it may play a positive role in other functions, including pathogenesis. The biological significance of the glycosylation of HEV capsid protein remains to be studied.

Although there is currently a lack of sensitive and reliable assays to determine the neutralizing activity of anti-HEV antibodies, the assay of NOB of HEV-LP binding to the target cells is thought to be a suitable alternative method. Measurement of the reactivity of a panel of mutant HEV-LPs revealed that the epitopes of MAB1323 and MAB272 antibodies are mapped in the peripheral region of the apical surface and the horizontal region of the P domain dimer, respectively. These results further support the notion that the P domain of HEV-LP is important for the binding to cells. MAB1323 is suggested to directly inhibit the interaction between HEV-LP and cellular receptors through binding to the apical surface, whereas MAB272 may have an allosteric effect, inducing conformational change of the P domain through binding to the horizontal region. A number of monoclonal antibodies are capable of neutralizing in vitro and in vivo infection of HEV (12–17), and many of them recognize conformational epitopes

of the capsid protein, as seen in the MAB1323 and MAB272 antibodies prepared in this study. Monoclonal antibodies against linear epitopes located in amino acids 578–607 of a genotype 1 capsid protein (16) were overlapped with a part of the putative receptor-binding domain and the epitope of MAB272, supporting the data of the present study. On the other hand, monoclonal antibodies against the linear epitopes located in amino acids 423–438 and amino acids 423–443 in the M domain of a genotype 1 capsid protein neutralized binding of a peptide derived from the capsid protein to cells and HEV-infection (13), suggesting the importance of the M domain in the binding step.

In summary, we have determined the crystal structure of HEV-LP produced in insect cells and demonstrated its structural characteristics in comparison with the structurally related animal and plant viruses. This study will provide useful information for elucidation of the molecular mechanisms of HEV-life cycles and for the development of prophylactic and therapeutic measures for hepatitis E.

Materials and Methods

Expression, Purification, and Crystallization of HEV-LP. The recombinant baculovirus encoding the ORF2 of the HEV genotype 3, 2712 strain was expressed in insect cells. HEV-LP was purified as described previously (28) and crystallized by the hanging-drop vapor-diffusion method. Details are reported in *SI Materials and Methods*.

Data Collection and Phase Determination. x-ray diffraction data were collected at 100 K on beamlines BL17A at the Photon Factory (KEK). The statistics of X-ray diffraction data collection are summarized in Table 1. The solved 3D structure of HEV-LP was submitted to the Protein Data Bank under the PDB accession code of 2ZTN. Details are reported in *SI Materials and Methods*.

ACKNOWLEDGMENTS. We thank H. Murase for her secretarial work and the staff of SPring-8 BL44XU beamline and synchrotron beamline NW-17A of the Photon Factory, High Energy Accelerator Research Organization for their assistance with the data collection. This work was supported in part by grants-in-aid from the Research and Development Program for New Bio-industry Initiatives of Bio-oriented Technology Research Advancement Institution (BRAIN) and the Foundation for Research Collaboration Center on Emerging and Re-emerging Infections.

1. Panda SK, Thakral D, Rehman S (2007) Hepatitis E virus. *Rev Med Virol* 17:151–180.
2. Purcell RH, Emerson SU (2008) Hepatitis E: An emerging awareness of an old disease. *J Hepatol* 48:494–503.
3. Navaneethan U, Al Mohajer M, Shata MT (2008) Hepatitis E and pregnancy: Understanding the pathogenesis. *Liver Int* 28:1190–1199.
4. Meng XJ, *et al.* (1997) A novel virus in swine is closely related to the human hepatitis E virus. *Proc Natl Acad Sci USA* 94:9860–9865.
5. Sonoda H, *et al.* (2004) Prevalence of hepatitis E virus (HEV) infection in wild boars and deer and genetic identification of a genotype 3 HEV from a boar in Japan. *J Clin Microbiol* 42:5371–5374.
6. Okamoto H (2007) Genetic variability and evolution of hepatitis E virus. *Virus Res* 127:216–228.
7. Li TC, *et al.* (2005) Hepatitis E virus transmission from wild boar meat. *Emerg Infect Dis* 11:1958–1960.
8. Yazaki Y, *et al.* (2003) Sporadic acute or fulminant hepatitis E in Hokkaido, Japan, may be food-borne, as suggested by the presence of hepatitis E virus in pig liver as food. *J Gen Virol* 84:2351–2357.
9. Tam AW, *et al.* (1991) Hepatitis E virus (HEV): Molecular cloning and sequencing of the full-length viral genome. *Virology* 185:120–131.
10. Matsubayashi K, *et al.* (2004) Transfusion-transmitted hepatitis E caused by apparently indigenous hepatitis E virus strain in Hokkaido, Japan. *Transfusion* 44:934–940.
11. Huang FF, *et al.* (2004) Determination and analysis of the complete genomic sequence of avian hepatitis E virus (avian HEV) and attempts to infect rhesus monkeys with avian HEV. *J Gen Virol* 85:1609–1618.
12. Emerson SU, *et al.* (2006) Putative neutralization epitopes and broad cross-genotype neutralization of Hepatitis E virus confirmed by a quantitative cell-culture assay. *J Gen Virol* 87:697–704.
13. He S, *et al.* (2008) Putative receptor-binding sites of hepatitis E virus. *J Gen Virol* 89:245–249.
14. Meng J, *et al.* (2001) Identification and characterization of the neutralization epitope(s) of the hepatitis E virus. *Virology* 288:203–211.
15. Takahashi M, *et al.* (2008) Production of monoclonal antibodies against hepatitis E virus capsid protein and evaluation of their neutralizing activity in a cell culture system. *Arch Virol* 153:657–666.
16. Schofield DJ, Glamann J, Emerson SU, Purcell RH (2000) Identification by phage display and characterization of two neutralizing chimpanzee monoclonal antibodies to the hepatitis E virus capsid protein. *J Virol* 74:5548–5555.
17. Schofield DJ, Purcell RH, Nguyen HT, Emerson SU (2003) Monoclonal antibodies that neutralize HEV recognize an antigenic site at the carboxyterminus of an ORF2 protein vaccine. *Vaccine* 22:257–267.
18. Graff J, *et al.* (2008) Mutations within potential glycosylation sites in the capsid protein of hepatitis E virus prevent the formation of infectious virus particles. *J Virol* 82:1185–1194.
19. Zafrullah M, Ozdener MH, Kumar R, Panda SK, Jameel S (1999) Mutational analysis of glycosylation, membrane translocation, and cell surface expression of the hepatitis E virus ORF2 protein. *J Virol* 73:4074–4082.
20. Huang R, *et al.* (1999) Cell culture of sporadic hepatitis E virus in China. *Clin Diagn Lab Immunol* 6:729–733.
21. Kazachkov Yu A, *et al.* (1992) Hepatitis E virus in cultivated cells. *Arch Virol* 127:399–402.
22. Meng J, Dubreuil P, Pillot J (1997) A new PCR-based seroneutralization assay in cell culture for diagnosis of hepatitis E. *J Clin Microbiol* 35:1373–1377.
23. Tam AW, *et al.* (1997) In vitro infection and replication of hepatitis E virus in primary cynomolgus macaque hepatocytes. *Virology* 238:94–102.
24. Tanaka T, Takahashi M, Kusano E, Okamoto H (2007) Development and evaluation of an efficient cell-culture system for Hepatitis E virus. *J Gen Virol* 88:903–911.
25. Bradley D, *et al.* (1988) Aetiological agent of enterically transmitted non-A, non-B hepatitis. *J Gen Virol* 69:731–738.
26. Li TC, *et al.* (1997) Expression and self-assembly of empty virus-like particles of hepatitis E virus. *J Virol* 71:7207–7213.
27. Li TC, *et al.* (2005) Essential elements of the capsid protein for self-assembly into empty virus-like particles of hepatitis E virus. *J Virol* 79:12999–13006.
28. Xing L, *et al.* (1999) Recombinant hepatitis E capsid protein self-assembles into a dual-domain T = 1 particle presenting native virus epitopes. *Virology* 265:35–45.
29. Prasad BV, *et al.* (1999) X-ray crystallographic structure of the Norwalk virus capsid. *Science* 286:287–290.
30. Chen R, Neill JD, Estes MK, Prasad BV (2006) X-ray structure of a native calicivirus: Structural insights into antigenic diversity and host specificity. *Proc Natl Acad Sci USA* 103:8048–8053.
31. Morgunova E, *et al.* (1994) The atomic structure of Carnation Mottle Virus capsid protein. *FEBS Lett* 338:267–271.
32. Hogle JM, Chow M, Filman DJ (1985) Three-dimensional structure of poliovirus at 2.9 A resolution. *Science* 229:1358–1365.
33. Tsao J, *et al.* (1991) The three-dimensional structure of canine parvovirus and its functional implications. *Science* 251:1456–1464.
34. Bhella D, Gatherer D, Chaudhry Y, Pink R, Goodfellow IG (2008) Structural insights into calicivirus attachment and uncoating. *J Virol* 82:8051–8058.
35. Bu W, *et al.* (2008) Structural basis for the receptor binding specificity of Norwalk virus. *J Virol* 82:5340–5347.
36. Choi JM, Hutson AM, Estes MK, Prasad BV (2008) Atomic resolution structural characterization of recognition of histo-blood group antigens by Norwalk virus. *Proc Natl Acad Sci USA* 105:9175–9180.
37. Li TC, *et al.* (2004) Protection of cynomolgus monkeys against HEV infection by oral administration of recombinant hepatitis E virus-like particles. *Vaccine* 22:370–377.
38. Hsu C, *et al.* (2006) Characterization of polymorphism displayed by the coat protein mutants of tomato bushy stunt virus. *Virology* 349:222–229.
39. Kakani K, Reade R, Katpally U, Smith T, Rochon D (2008) Induction of particle polymorphism by cucumber necrosis virus coat protein mutants in vivo. *J Virol* 82:1547–1557.
40. White LJ, Hardy ME, Estes MK (1997) Biochemical characterization of a smaller form of recombinant Norwalk virus capsids assembled in insect cells. *J Virol* 71:8066–8072.
41. Belnap DM, *et al.* (2000) Molecular tectonic model of virus structural transitions: The putative cell entry states of poliovirus. *J Virol* 74:1342–1354.
42. Bubeck D, Filman DJ, Hogle JM (2005) Cryo-electron microscopy reconstruction of a poliovirus-receptor-membrane complex. *Nat Struct Mol Biol* 12:615–618.
43. Jayaram H, Estes MK, Prasad BV (2004) Emerging themes in rotavirus cell entry, genome organization, transcription and replication. *Virus Res* 101:67–81.

Supporting Information

Yamashita et al. 10.1073/pnas.0903699106

SI Materials and Methods

Cell Culture. The insect cell lines Sf9 and BTI-Tn-5B1–4 (Tn5) were maintained in Sf-900II medium (Invitrogen) supplemented with 10% FBS and Ex-cell 405 medium (JRH Biosciences), respectively. The human hepatoma cell lines, Huh7, PLC/PRF/5, HepG2, Hep3B, and FLC4, human alveolar epithelial A549 cells, and human embryonic kidney 293T cells were maintained in Dulbecco's modified Eagle's MEM (Sigma) supplemented with 10% FBS. Mouse myeloma P3U1 cells were grown in RPMI-1640 medium (Invitrogen) supplemented with 10% FBS.

Production of Anti-HEV-LP Monoclonal Antibodies. Hybridoma cells producing anti-HEV-LP monoclonal antibodies were generated at Bio Matrix Research by the standard method. All of 11 monoclonal antibodies (IgG1 or IgG2a isotypes) were confirmed to be capable of detecting HEV-LP on ELISA. These antibodies were purified by an affinity chromatography using protein G columns. Among them, MAB358, MAB1323, and MAB272 were biotinylated for use in the neutralization of cell-binding assay and competitive ELISA.

Expression of HEV Capsid Protein and Purification of HEV-LP. The recombinant baculovirus AcMNPV encoding amino acid residues 112 to 608 of the ORF2 of the HEV genotype 3, 2712 strain was produced by a Bacmid-based method (Invitrogen) following the manufacturer's instructions. To prepare a series of mutants of the HEV capsid protein in which asparagine was replaced with alanine at the residue 200 (N200A), or tyrosine was replaced with other amino acids at residue 288 (Y288A, Y288W, Y288F, Y288L, Y288D, Y288H, and Y288R), or surface amino acids of the P domain were replaced with alanines, the corresponding nucleotide mutations were introduced into pFastBac1 vector (Invitrogen) encoding the wild-type HEV ORF2 by a site-directed mutagenesis based on PCR (1). The virus stock was propagated in Sf9 cells and HEV-LP was expressed in Tn5 cells. HEV-LP was purified and particle formation was determined by a discontinuous sucrose gradient centrifugation as described previously (2). For immunoprecipitation and cell-binding analyses, the HEV-LP-containing fractions were dialyzed with PBS and concentrated to 200 μg/mL.

Crystallization of HEV-LP. Crystallizations were performed using the hanging-drop vapor-diffusion method at 293 K using the conditions described previously (3). The best crystals of HEV-LP were obtained with 6% (wt/vol) PEG 10,000 and 35% (wt/vol) ethylene glycol in 100 mM Tris-HCl buffer (pH 8.0). The droplets consisted of equal volumes (3 μL) of protein solution and reservoir solution.

Data Collection and Processing. The crystals of HEV-LP were mounted in nylon CryoLoops (Hampton Research) and placed directly into a nitrogen stream at 100 K. X-ray diffraction data were collected at 100 K on beamlines BL17A (wavelength 1.0000 Å) at the Photon Factory (KEK) using an ADSC Quantum 270 CCD detector. Oscillation data were recorded in frames of 0.3 oscillation with 30-s exposure time per image. The complete data set was merged with 3 crystal data sets. The collected data were processed with the program *HKL-2000* (4). The statistics of X-ray diffraction data collection are summarized in Table 1. The space groups of HEV-LP crystals were determined to be orthorhombic $P2_12_12_1$. Assuming the presence of 1 molecule of HEV-LP in the asymmetric unit, the value of the Matthews coefficient V_M (5) was 3.31 Å^3 Da^{-1}, corresponding to a solvent content of 62.8%, both of which were within the normal range of values for protein crystals (5). The self-rotation functions showed pronounced peaks indicating 2-fold, 3-fold, and 5-fold noncrystallographic rotation symmetry. The calculation of the Matthews coefficient is based on the reasonable assumption of a T = 1 particle.

Phase Determination. The self-rotation function was computed with the program *POLARRFN* of the *CCP4* package (6) to determine the orientation of icosahedral noncrystallographic symmetry elements. The particle orientation in the unit cell and particle position were determined by a self-rotation function and translation search with the crystal structure of HEV-LP genotype 1 which was previously determined at 8.3-Å resolution (3), respectively. By using the data in the range of 50–20-Å resolution, the maximum correlation coefficient and the minimum R-factor values were determined as 0.642 and 0.363, respectively. The particle orientation and position of HEV-LP of genotype 3 in the crystal were slightly different from those of genotype 1 (3), which resulted in the different length of the cell axes with the same space group ($P2_12_12_1$). Phase refinement and extension were carried out to the resolution of 3.5 Å as described previously (3). The final correlation coefficient and R-factor between the F_os and the F_cs obtained from inversion of the averaged and solvent-flattened map at 3.5 Å resolution were 0.928 and 0.235, respectively. The electron density map was of good quality and allowed interpretation in terms of the secondary and tertiary structures of the subunits. We built an atomic model into the electron density map using the program O (7), and the model was refined using the program CNS. We calculated the electrostatic potentials of HEV-LP by the *GRASP* program (7). The solved 3D structure of HEV-LP was submitted to the Protein Data Bank under the PDB accession code of 2ZTN.

Cell-Binding Assay. Cultured cells (5×10^5 cells)were detached with 2 mM EDTA and incubated with 100 μL HEV-LP (10 μg/mL) for 1 h at 4°C. After being washed twice with PBS containing 0.35% BSA, the cells were fixed with 0.5% paraformaldehyde for 15 min at 4°C. After further washing, HEV-LPs bound to cells were stained with anti-HEV-LP MAB358 and Alexa Flour 488-labeled goat anti-mouse IgG antibodies (Invitrogen), and analyzed by a BD FACSCalibur flow cytometry system (BD). For neutralization of binding of HEV-LP to cells, 100 μL HEV-LP (10 μg/mL) was preincubated with anti-HEV-LP monoclonal antibodies (20 μg/mL) for 1 h at 37°C before incubation with cells, and bound HEV-LPs were stained with biotinylated MAB358 and phycoerythrin-conjugated streptavidin (BD PharMingen).

Immunoprecipitation. The wild-type and mutant HEV-LPs (200 ng/mL) were incubated with Protein G Sepharose 4 Fast Flow beads (GE Healthcare) for 1 h at 4°C. After centrifugation, 0.5 μg anti-HEV-LP monoclonal antibodies were added to the supernatants. After incubation for 1 h at 4°C, 15 μL Protein G beads was added and the solution was further incubated for 1 h at 4°C. The beads were washed 5 times with PBS containing 0.5% Tween20, suspended in 30 μL SDS/PAGE sample buffer and boiled for 5 min. The samples were analyzed by western blotting using an anti-HEV-LP rabbit polyclonal antibody.

1. Higuchi R, Krummel B, Saiki RK (1988) A general method of in vitro preparation and specific mutagenesis of DNA fragments: Study of protein and DNA interactions. *Nucleic Acids Res* 16:7351–7367.
2. Xing L, *et al.* (1999) Recombinant hepatitis E capsid protein self-assembles into a dual-domain T = 1 particle presenting native virus epitopes. *Virology* 265:35–45.
3. Wang CY, *et al.* (2008) Crystallization and preliminary X-ray diffraction analysis of recombinant hepatitis E virus-like particle. *Acta Crystallogr Sect F Struct Biol Cryst Commun* 64:318–322.
4. Otwinowski Z, Minor W (1997) Processing of X-ray diffraction data collected in oscillation mode. *Methods in Enzymology* 276:307–326.
5. Matthews BW (1968) Solvent content of protein crystals. *J Mol Biol* 33:491–497.
6. Collaborative Computational Project N (1994) The CCP4 suite: Programs for protein crystallography. *Acta Crystallogr D Biol Crystallogr* 50:760–763.
7. Nicholls A, Sharp KA, Honig B (1991) Protein folding and association: Insights from the interfacial and thermodynamic properties of hydrocarbons. *Proteins* 11:281–296.

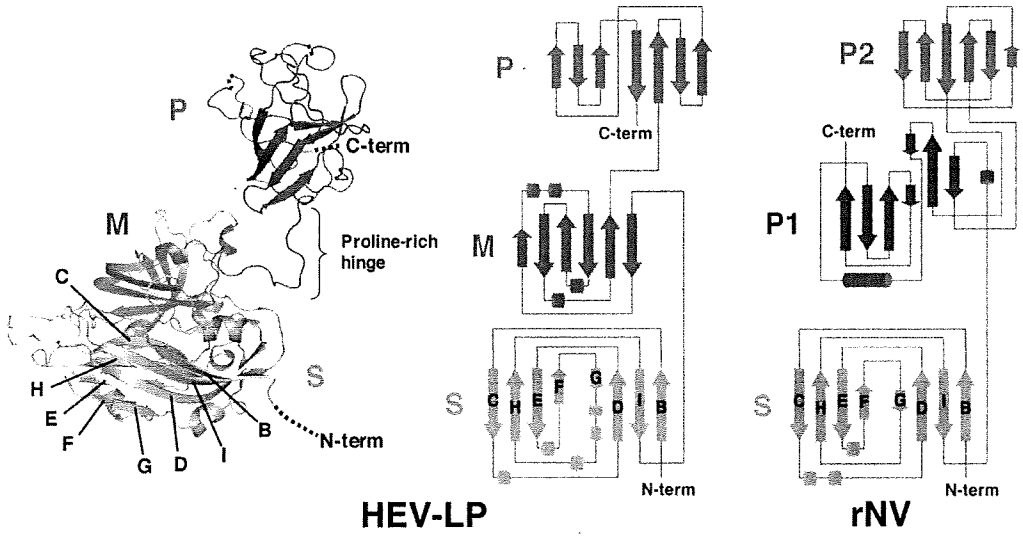

Fig. S1. Capsid monomers of HEV-LP and rNV. The ribbon diagram of a capsid monomer of HEV-LP is indicated in the left. The respective topology diagrams of capsid monomers from HEV-LP and recombinant Norwalk virus (rNV) are indicated. The S, M, and P domains of the HEV-LP capsid protein are indicated by pink, green and blue, respectively. The S, P1, and P2 domains of the rNV capsid protein are indicated by pink, dark blue, and blue, respectively. The β-strands and α-helices are shown with arrows and tubes, respectively.

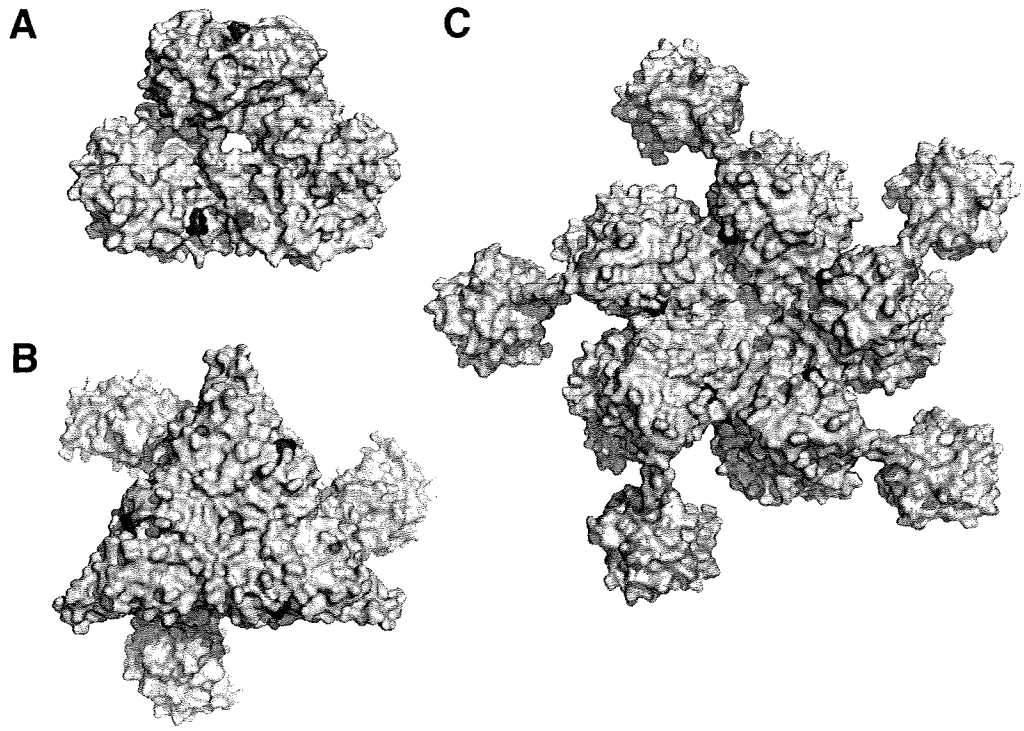

Fig. S2. Three-dimensional mapping of potential *N*-glycosylation sites at dimer (*A*), trimer (*B*), and pentamer (*C*) structures of the capsid protein in HEV-LP. Asparagine residues of possible *N*-glycosylation sites, Asn-137-Leu-Ser, Asn-310-Leu-Thr, and Asn-562-Thr-Thr, are colored red, orange, and blue, respectively, on the surface diagrams from a lateral (*A*) or inside (*B* and *C*) view. The S, M, and P domains are indicated in pink, blue, and gray, respectively.

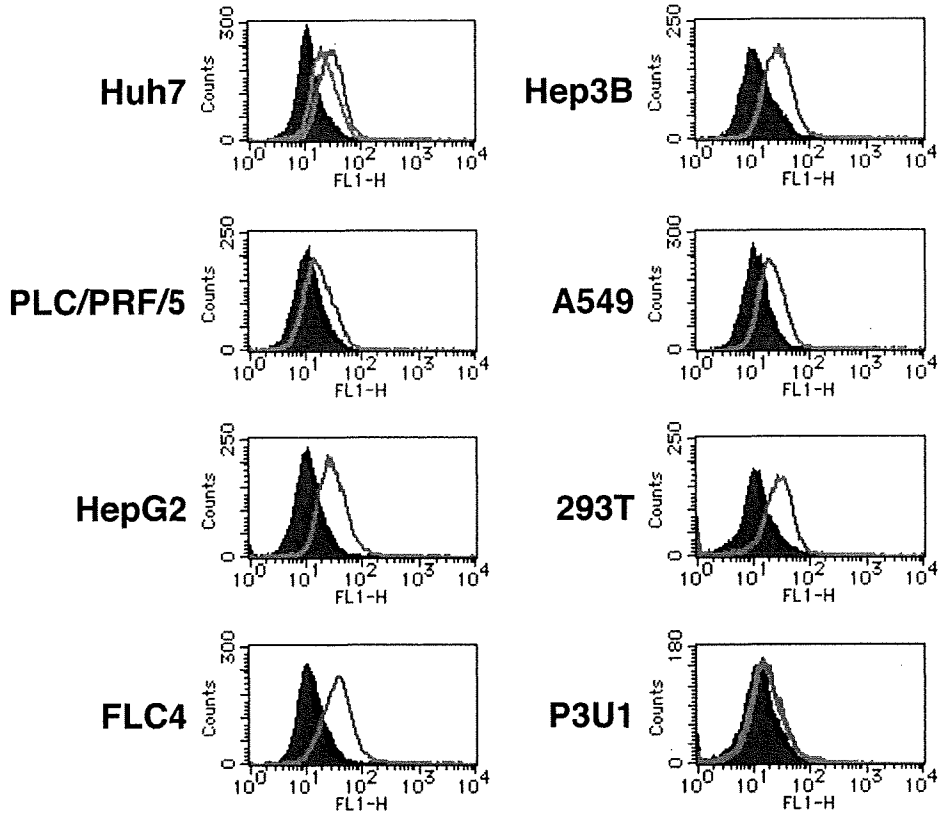

Fig. S3. HEV-LP binding to culture cells. HEV-LPs were incubated with the indicated cells for 1 h at 4°C, and then HEV-LPs bound to cells were detected by flow cytometry. The blue and green lines indicate incubation with 1 and 10 μg/mL HEV-LPs, respectively. The filled area indicates mock-incubated cells.

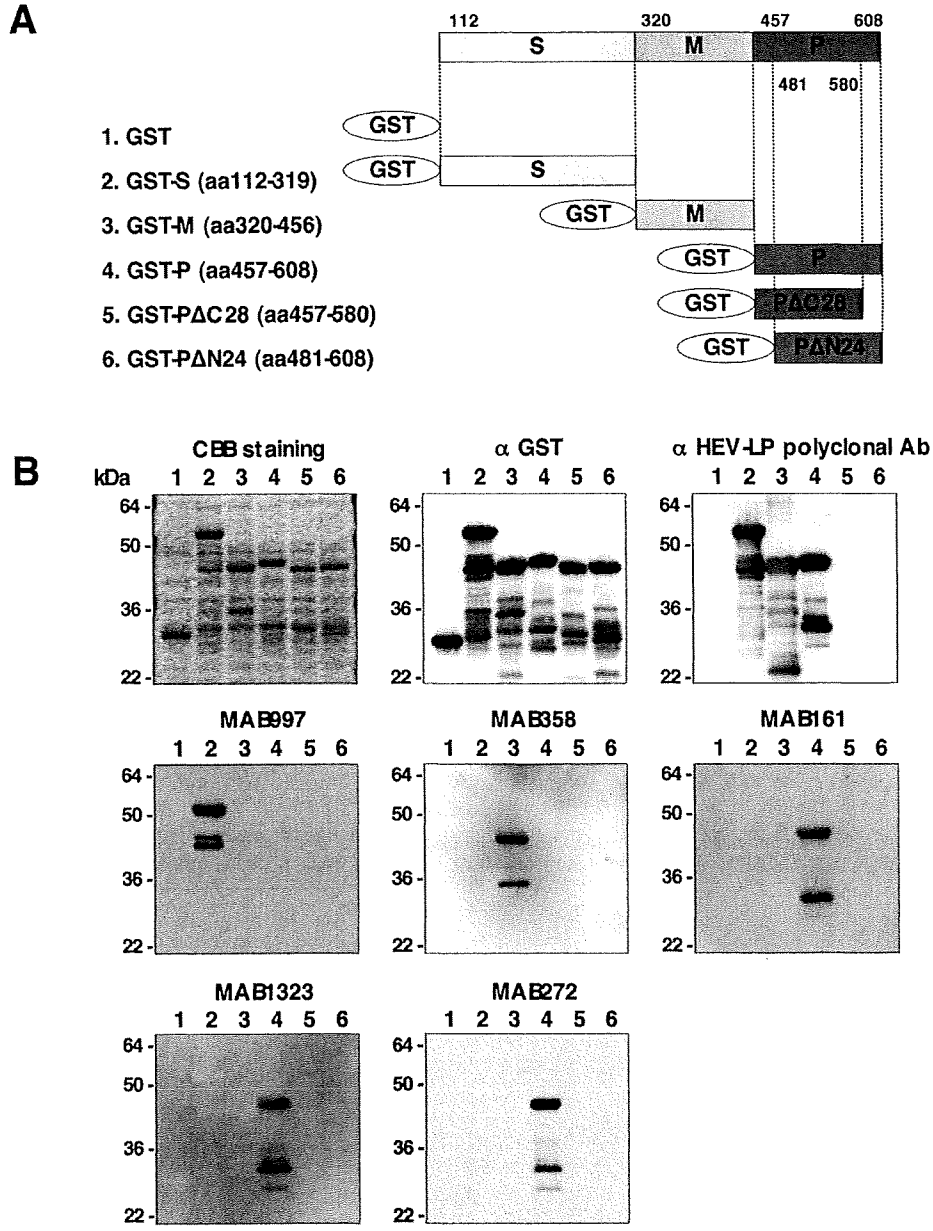

Fig. S4. Determination of HEV-LP subdomain recognized by anti-HEV-LP antibodies. (*A*) Schematic representation of GST or GST-fused HEV-LP subdomains used for epitope mapping. The cDNAs encoding the indicated amino acid residues were introduced into a pGEX-4T3 vector and were expressed as GST-fused proteins in bacteria. (*B*) The lysates of cells expressing GST or GST-fused proteins were applied to SDS/PAGE and stained with Coomassie Brilliant Blue (CBB) or examined by immunoblotting with polyclonal and monoclonal antibodies. The lane numbers correspond to those in *A*.

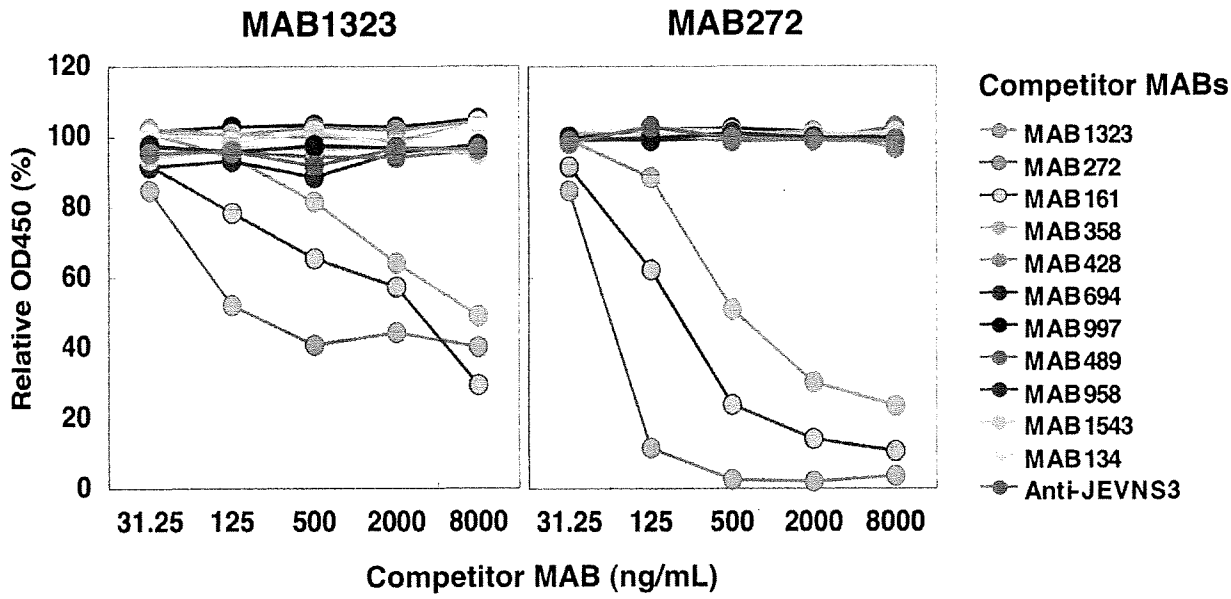

Fig. S5. Competitive ELISA of monoclonal antibodies to HEV-LP. The wild-type HEV-LP (50 or 100 ng/mL) was inoculated into wells of a 96-well-immuno-plate (Nunc) and incubated at 4°C overnight. Unbound HEV-LP was washed out with PBST 3 times and the wells were incubated with PBS containing 1% BSA. After washing, serially diluted competitor antibodies were reacted for 1 h at 25°C. After washing 5 times, biotinylated MAB1323 (500 ng/mL) or MAB272 (50 ng/mL) was reacted for 1 h at 25°C. Bound biotinylated antibodies were further reacted with horseradish peroxidase-conjugated streptavidin (Vector) and visualized with 3, 3′, 5, 5′-tetramethyl-benzidene (Nacalai Tesque). Optical densities of 450 nm in the wells without competitor antibodies were defined as 100% reactivity.

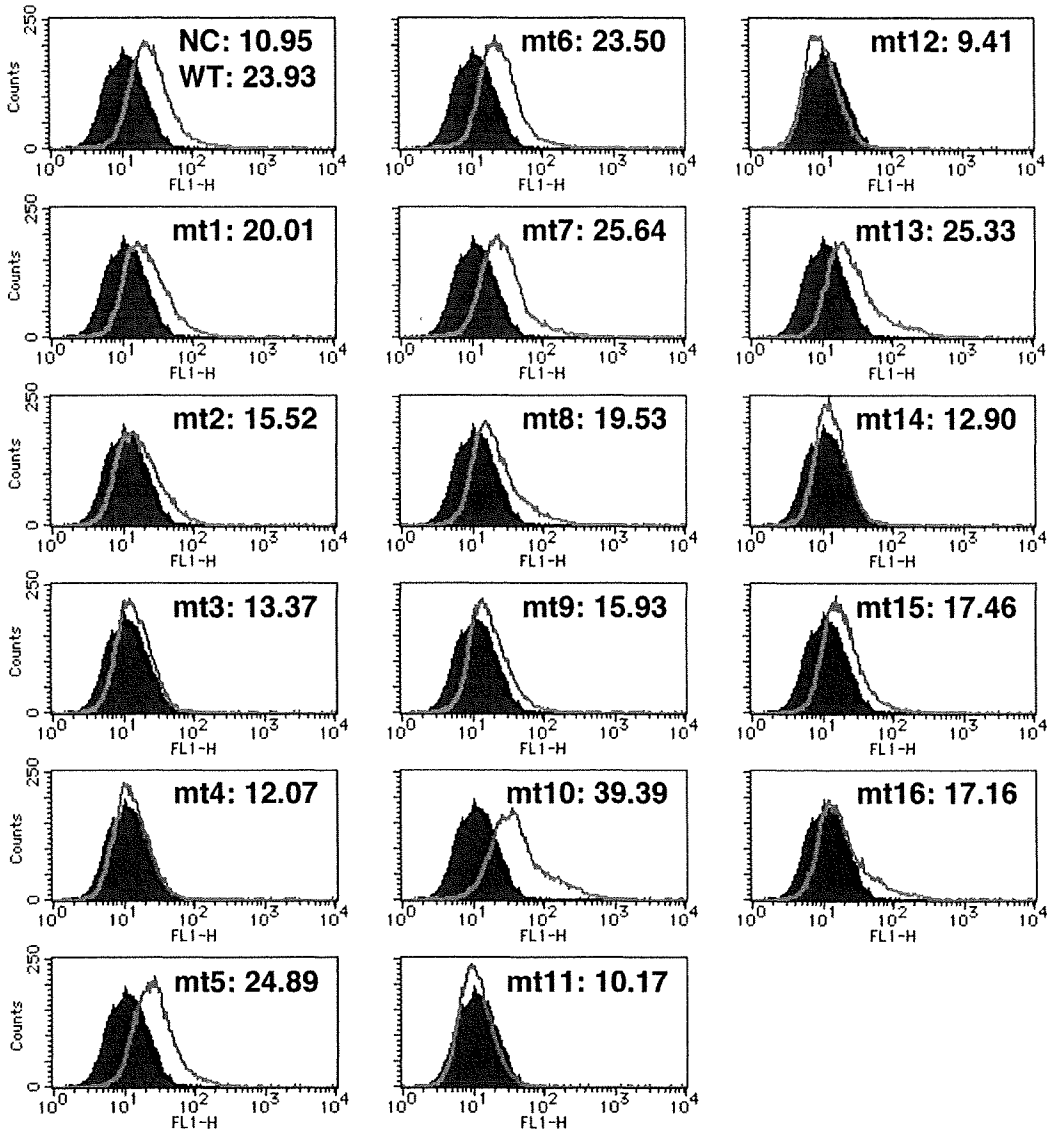

Fig. S6. Binding of HEV-LP mutants to A549 cells. Wild-type and mutant HEV-LPs (10 μg/mL) were incubated with A549 cells for 1 h at 4°C, and HEV-LP bound to cells (lined area) were detected by flow cytometry. The filled area indicates mock-incubated cells. The MFI is also indicated in each panel.

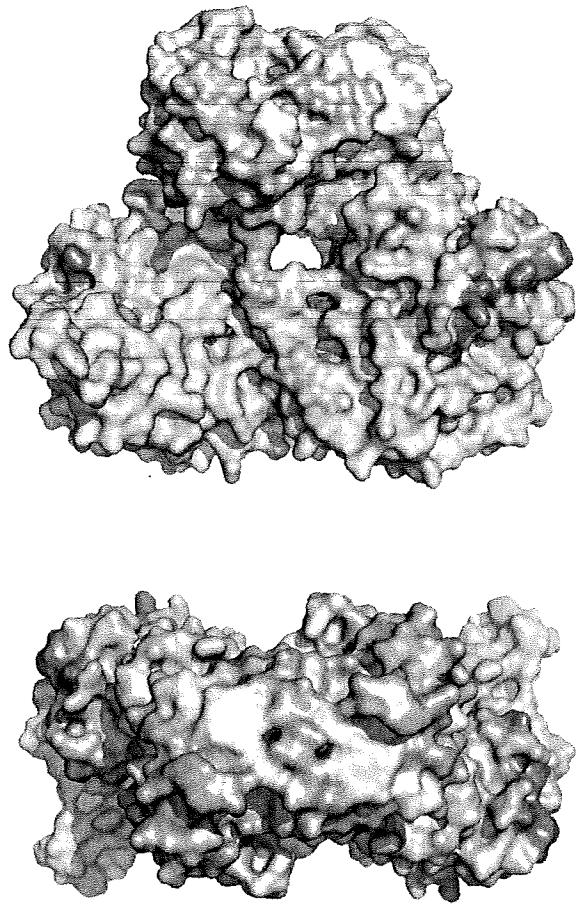

Fig. S7. Three-dimensional mapping of epitopes for neutralizing antibodies against genotype 1 strains previously reported. Surface diagrams of capsid protein dimer from a lateral (upper) or top (lower) view. The regions containing linear epitopes for the neutralizing antibodies HEV#4 and #31 (amino acids 578–607) reported by Schofield et al. (16) were colored yellow, while those of 12A10 (amino acids 423–438) and 16D7 (amino acids 423–443) reported by He et al. (13) were colored brown. Domains S, M, and P are colored pink, blue, and gray, respectively.

JOURNAL OF VIROLOGY, Aug. 2009, p. 7959–7969 Vol. 83, No. 16
0022-538X/09/$08.00+0 doi:10.1128/JVI.00889-09

Human VAP-C Negatively Regulates Hepatitis C Virus Propagation▽

Hiroshi Kukihara,[1] Kohji Moriishi,[1] Shuhei Taguwa,[1] Hideki Tani,[1] Takayuki Abe,[1] Yoshio Mori,[1] Tetsuro Suzuki,[2] Takasuke Fukuhara,[1,3] Akinobu Taketomi,[3] Yoshihiko Maehara,[3] and Yoshiharu Matsuura[1]*

Department of Molecular Virology, Research Institute for Microbial Diseases, Osaka University, Osaka,[1] Department of Virology II, National Institute of Infectious Diseases, Tokyo,[2] and Department of Surgery and Science, Graduate School of Medical Sciences, Kyushu University, Fukuoka,[3] Japan

Received 3 May 2009/Accepted 2 June 2009

Human vesicle-associated membrane protein-associated protein (VAP) subtype A (VAP-A) and subtype B (VAP-B) are involved in the regulation of membrane trafficking, lipid transport and metabolism, and the unfolded protein response. VAP-A and VAP-B consist of the major sperm protein (MSP) domain, the coiled-coil motif, and the C-terminal transmembrane anchor and form homo- and heterodimers through the transmembrane domain. VAP-A and VAP-B interact with NS5B and NS5A of hepatitis C virus (HCV) through the MSP domain and the coiled-coil motif, respectively, and participate in the replication of HCV. VAP-C is a splicing variant of VAP-B consisting of the N-terminal half of the MSP domain of VAP-B followed by the subtype-specific frameshift sequences, and its biological function has not been well characterized. In this study, we have examined the biological functions of VAP-C in the propagation of HCV. VAP-C interacted with NS5B but not with VAP-A, VAP-B, or NS5A in immunoprecipitation analyses, and the expression of VAP-C inhibited the interaction of NS5B with VAP-A or VAP-B. Overexpression of VAP-C impaired the RNA replication of the HCV replicon and the propagation of the HCV JFH1 strain, whereas overexpression of VAP-A and VAP-B enhanced the replication. Furthermore, the expression of VAP-C was observed in various tissues, whereas it was barely detected in the liver. These results suggest that VAP-C acts as a negative regulator of HCV propagation and that the expression of VAP-C may participate in the determination of tissue tropism of HCV propagation.

Hepatitis C virus (HCV) is a major causative agent of chronic liver disease and thus a major public health problem, infecting at least 3% of the world population (47). HCV infection proceeds to the persistent stage in approximately 80% of patients, leading to the development of cirrhosis in 20% to 50% of patients, of whom approximately 5% eventually develop hepatocellular carcinoma (12). HCV encompasses a single-stranded positive-sense RNA genome of approximately 9.6 kb, which encodes a large precursor polyprotein comprising approximately 3,000 amino acids (26). The structural proteins are cleaved from the N-terminal one-fourth of the polyprotein by the host signal peptidase and signal peptide peptidase (23, 32, 33), resulting in the maturation of the capsid protein, two envelope proteins and viroporin p7. The NS2 protease cleaves after the carboxyl terminus, and then NS3 cleaves the appropriate downstream positions to produce NS4A, NS4B, NS5A, and NS5B (8, 42), all of which form the replication complex along with several host proteins (5, 21). NS5B is the RNA-dependent RNA polymerase, which is a main enzymatic component of the replication complex of HCV (3), while NS5A is a membrane-anchored zinc-binding phosphoprotein that appears to possess diverse functions, including the suppression of host defense and the regulation of the virus's replication (1, 4, 6, 41), although its biological function remains unclear.

The NS5A protein has been shown to interact with several host proteins, including vesicle-associated membrane protein (VAMP)-associated protein (VAP) subtype A (VAP-A) (44) and subtype B (VAP-B) (9), FKBP8 (34), MyD88 (1), FBL2 (46), human butyrate-induced transcript 1 (hB-ind1) (40), and so on (25). VAP-A and VAP-B also bind to NS5B, although it remains unclear whether these interactions modulate HCV replication positively or negatively (9, 44). VAP-A and VAP-B have been shown to associate with the cytoplasmic face of the endoplasmic reticulum (ER) and the Golgi apparatus (38) and to consist of the major sperm protein (MSP) domain, the coiled-coil domain, and the transmembrane (TM) region, in that order (30, 39), as shown in Fig. 1A. VAP was originally reported as a protein binding to VAMP, which is a synaptic vesicle SNARE protein required for synaptic-vesicle fusion in the nematode *Aplysia californica*, and was designated the 33-kDa VAMP-associated protein, VAP-33 (39). Two mammalian homologues, VAP-A and VAP-B, were subsequently identified (30, 38). The transcription of VAP-A and VAP-B is ubiquitously detected in mammalian organs, including the heart, placenta, lung, liver, skeletal muscle, and pancreas (30), suggesting that VAP family proteins are involved in diverse cellular functions other than neurotransmitter release (30, 38, 49). Several VAP-interacting proteins share the FFAT motif (two phenylalanines in an acidic tract), which has the consensus amino acid sequence EFFDAXE, as determined by a comparison among oxysterol binding proteins (OSBPs), OSBP-related proteins (ORPs) (20), and the ceramide transport protein CERT (10, 19), contributing to the regulation of fatty acid metabolism. The interaction of VAP family proteins with

* Corresponding author. Mailing address: Department of Molecular Virology, Research Institute for Microbial Diseases, Osaka University, 3-1, Yamadaoka, Suita, Osaka 565-0871, Japan. Phone: 81-6-6879-8340. Fax: 81-6-6879-8269. E-mail: matsuura@biken.osaka-u.ac.jp.
▽ Published ahead of print on 10 June 2009.

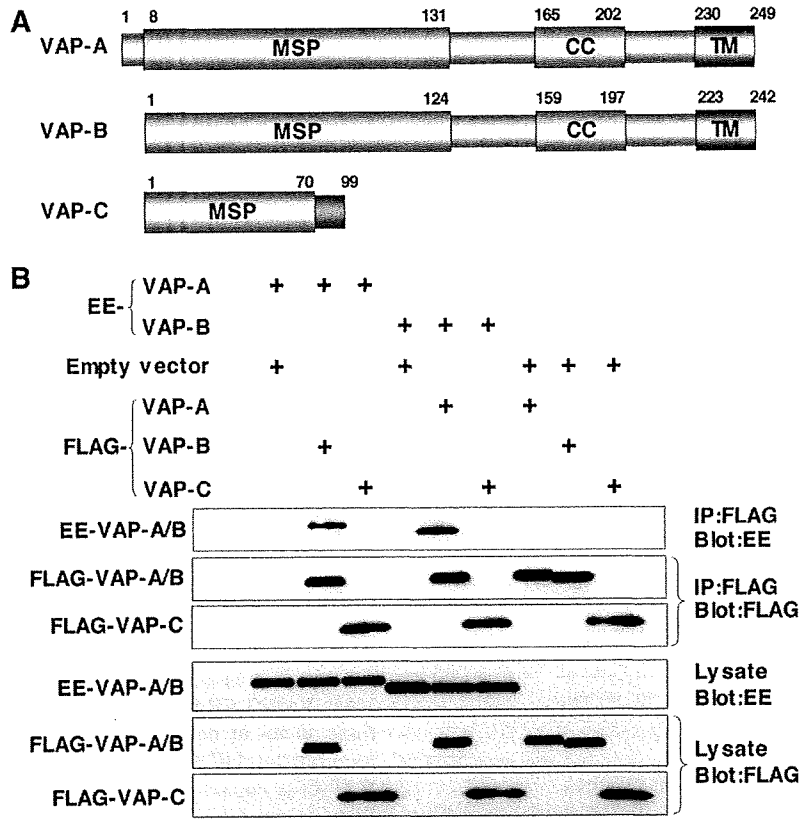

FIG. 1. VAP-C interacts with neither VAP-A nor VAP-B. (A) Structures of VAP family proteins. The MSP domain, the coiled-coil domain, and the TM region are indicated as MSP, CC, and TM, respectively. (B) Interaction among VAP family proteins. The expression plasmids encoding VAP proteins or empty vector (1 μg each) were transfected into 293T cells, FLAG-tagged VAP proteins coexpressed with EE-tagged VAP-A or VAP-B were immunoprecipitated (IP) with anti-FLAG antibody, and the resulting precipitates were examined by immunoblotting using anti-FLAG or anti-EE antibody. One percent of the volume of the lysate was used as an input control. The data in each panel are representative of the results of three independent experiments. +, present.

other host proteins, including VAMP and tubulin, is independent of the FFAT motif (16, 36, 38, 50). The third subtype of VAP is VAP-C, which is an alternative spliced isoform of VAP-B, consisting of the N-terminal half of the MSP domain and the subtype-specific 29 amino acids (Fig. 1A). However, its tissue distribution and physiological function remain largely unknown.

Glutathione *S*-transferase pulldown and immunoprecipitation analyses revealed that both VAP-A and VAP-B interact with NS5B and NS5A through the MSP domain and the coiled-coil domain, respectively (9, 44), and the MSP domains of VAP-A and VAP-B exhibit 82.3% homology. Although VAP-C possesses the N-terminal-half region of the MSP domain of VAP-B, the biological significance of VAP-C in the propagation of HCV has not yet been clarified. In this study, we examined the expression of VAP-C in human tissues and the effects of VAP-C expression on the RNA replication, translation, and particle formation of HCV.

MATERIALS AND METHODS

Cell lines. Cells of the human hepatoma cell line Huh-7, cell line Huh7OK1, and embryonic kidney cell line 293T were maintained in Dulbecco's modified Eagle's medium (DMEM) (Sigma, St. Louis, MO) containing 10% fetal calf serum (FCS) and nonessential amino acids (NEAA), while Huh 9-13 cells, which possess a subgenomic HCV RNA replicon of genotype 1b (21), were cultured in DMEM supplemented with 10% FCS, NEAA, and 1 mg/ml G418. The Huh7OK1 cell line exhibits the highest efficiency of propagation of strain JFH1 virus, as described previously (35). All cell lines were cultured at 37°C in a humidified atmosphere with 5% CO_2.

Antibodies. Chicken anti-human VAP-B antibody was described previously (9). Rabbit anti-human VAP-C antibody was prepared by immunization using synthetic peptides of the amino acid residues from 86 to 98, QPHFSISPNW EGR, which region does not share the homology to VAP-A and VAP-B. The mouse monoclonal antibody to human VAP-A was purchased from BD Pharmingen (San Diego, CA). Mouse monoclonal antibodies to influenza virus hemagglutinin (HA) and the GluGlu (EE) tag were from Covance (Richmond, CA). Mouse and rabbit anti-FLAG antibodies and mouse anti-β-actin monoclonal antibody were from Sigma. Rabbit polyclonal antibody to NS5A was prepared as described previously (34). Mouse anti-NS5A monoclonal antibody was from Austral Biologicals (San Ramon, CA).

Plasmids. A cDNA clone encoding NS5A was amplified from HCV genotype 1b strain J1 (9) (GenBank database accession number D89815) by PCR, using *Pfu* turbo DNA polymerase (Stratagene, La Jolla, CA). The fragments were then cloned into the appropriate sites in pEF-FLAG pGBK puro (13). The DNA fragment encoding NS5B of the J1 strain was generated by PCR and cloned into pCAGGs-PUR (31). The DNA fragment encoding human VAP-A was amplified by PCR from a human fetal-brain library (Clontech, Palo Alto, CA) and was introduced into pEF-FLAG pGBK puro and pEF-EE hygro (13), as described previously (9). A DNA fragment encoding VAP-C was amplified from cDNA of hepatoma cell line Huh-7 and was introduced into pEF-FLAG pGBK puro. Pro^{56}-to-Ser (P56S) mutants of VAPs were generated by site-directed mutagen-

esis (11). All PCR products were confirmed by sequencing with an ABI Prism 3130 genetic analyzer (Applied Biosystems, Tokyo, Japan).

Transfection, immunoblotting, and immunoprecipitation. Cells were seeded onto a six-well tissue culture plate 24 h before transfection. The plasmids were transfected into cells by liposome-mediated transfection using TransIT LT1 (Mirus Bio, Madison, WI). These transfected cells were harvested at 36 h post-transfection, washed three times with 1 ml of ice-cold phosphate-buffered saline (PBS), and suspended in 0.2 ml lysis buffer (20 mM Tris-HCl, pH 7.4, containing 135 mM NaCl and 1% Triton X-100) supplemented with protease inhibitor cocktail (Roche, Indianapolis, IN). The cell lysates were sonicated at 4°C for 5 min, incubated for 30 min at 4°C, and centrifuged at 15,000 rpm for 30 min at 4°C. The supernatant was subjected to immunoprecipitation analyses as described previously (27). The immunoprecipitated proteins were boiled in 30 μl of loading buffer and then subjected to sodium dodecyl sulfate–12.5% polyacrylamide gel electrophoresis. The proteins were transferred to polyvinylidene difluoride membranes (Millipore, Bedford, MA) and then reacted with primary antibody and secondary horseradish peroxidase-conjugated antibody. The immunocomplexes were visualized with Super Signal West Femto substrate (Pierce, Rockford, IL) and detected by using an LAS-3000 image analyzer (Fujifilm, Tokyo, Japan). The distribution of VAPs in human organs was determined by using premade human tissue lysates (Protein medleys; Clonetech), which are aliquots of various organ lysates prepared from samples from several people, and liver tissues obtained during surgery after approval of the ethical committee of Kyushu University Graduate School of Medicine.

Real-time PCR. The HCV genomic RNA was determined by the method described previously (40). Total RNA was prepared from cells by using an RNeasy mini kit (Qiagen, Tokyo, Japan). First-strand cDNA was synthesized using an RNA LA PCR kit (Takara Bio, Inc., Shiga, Japan) and random primers. Expression of the appropriate gene was estimated by using platinum SYBR green quantitative PCR SuperMix UDG (Invitrogen, Carlsbad, CA) according to the manufacturer's protocol. Fluorescent signals were estimated by using an ABI Prism 7000 system (Applied Biosystems). The 5′ untranslated region of HCV and the glyceraldehyde-3-phosphate dehydrogenase (GAPDH) mRNA were amplified using primer pairs described previously (40). The amount of HCV genomic RNA was normalized with that of GAPDH mRNA.

Focus-forming assay. The viral RNA of the JFH1 strain was introduced into the Huh7OK1 cell line according to the method of Zhong et al. (51). The culture supernatant was collected at 7 days posttransfection and used as the infectious HCV particles. Huh7OK1 cells in DMEM containing 10% FCS were seeded at 5×10^4 cells per well into a 24-well plate 12 h before infection. The cells were infected with the JFH1 strain at a multiplicity of infection (MOI) of 0.05 and incubated at 37°C for 2 h. The medium was replaced with fresh DMEM containing 10% FCS and NEAA at 2 h postinfection. The cells were fixed with 4% paraformaldehyde at 96 h postinfection and permeabilized with PBS containing 0.2% Triton X-100. These fixed and permeabilized cells were stained with the anti-NS5A mouse monoclonal antibody and Alexa Fluor (AF) 488-conjugated antibody to mouse immunoglobulin G (Molecular Probes, Eugene, OR). Clusters of infected cells stained with the NS5A antibody were derived from a single infectious focus, and virus titers were represented as focus-forming units/ml.

Quantification of the HCV core protein by ELISA. The HCV core protein was quantified by using an Ortho HCV antigen enzyme-linked immunosorbent assay (ELISA) test (Ortho Clinical Diagnostics, Tokyo, Japan) according to the manufacturer's instructions. To determine the intracellular expression of core protein, Huh7OK1 cells were infected with the infectious HCV particles described above, lysed with the lysis buffer on ice, and applied to the ELISA after 100- to 10,000-fold dilution with PBS. Total protein was quantified by using a Micro BCA protein assay reagent kit (Pierce). The intracellular and extracellular levels of expression of the core protein were normalized by the total amount of protein.

Effect of the VAP expression on the cap-independent translational activity of the viral IRES. The cDNA fragment encoding a firefly luciferase was excised from a pGL3 basic plasmid (Promega, Madison, WI) and introduced into the downstream region of the *Renilla* luciferase gene of pRL-CMV (cytomegalovirus) (Promega). Then, the cDNA fragments encoding the internal ribosome entry site (IRES) of the HCV strains Con1 and JFH1 were introduced between the *Renilla* and firefly luciferase genes, and the resulting plasmids were designated pRL-CMV-HCVCon1 and pRL-CMV-HCVJFH1, respectively (see Fig. 4A). The IRES region of HCV was replaced with that of poliovirus (PV) or encephalomyocarditis virus (EMCV), and the plasmids designated pRL-CMV-PV and pRL-CMV-EMCV, respectively (see Fig. 4B). Each reporter plasmid was introduced into Huh7OK1 cells that had been transfected with the expression plasmid encoding FLAG-green fluorescent protein (GFP), FLAG–VAP-A, FLAG–VAP-B, or FLAG–VAP-C 24 h previously, and cells were harvested at 48 h posttransfection. Luciferase activities in cells were measured by using a dual-luciferase reporter assay system (Promega). The activity of firefly luciferase was normalized with that of *Renilla* luciferase and represented as relative luciferase activity (RLU).

Indirect immunofluorescence assay. The Huh 9-13 cells were cultured on glass slides and transfected with the expression plasmids encoding FLAG-tagged VAPs, P56S VAP mutants, or empty vector. The resulting cells were fixed at 72 h posttransfection with 4% paraformaldehyde in PBS at room temperature for 30 min. After being washed twice with PBS, cells were permeabilized for 20 min at room temperature with PBS containing 0.25% saponin and blocked with PBS containing 1% bovine serum albumin (BSA-PBS) for 60 min at room temperature. The cells were then incubated with BSA-PBS containing rabbit anti-FLAG and mouse anti-NS5A antibodies at 37°C for 60 min, washed three times with PBS containing 1% Tween 20 (PBS-T), and incubated with BSA-PBS containing AF 488-conjugated goat anti-rabbit immunoglobulin G and AF 594-conjugated goat anti-mouse antibodies at 37°C for 60 min. Finally, the cells were washed three times with PBS-T and observed with a FluoView FV1000 laser-scanning confocal microscope (Olympus, Tokyo, Japan).

RESULTS

VAP-C interacts with neither VAP-A nor VAP-B. The length of VAP-A was originally reported to be 242 amino acids but was recently corrected to 249 amino acids in the GenBank database due to the detection of 7 extra amino acids in the N terminus (Fig. 1A). VAP-C is a splicing variant of VAP-B that shares the N-terminal half of the MSP domain with VAP-B but lacks the coiled-coil motif and TM region (Fig. 1A). The region spanning residues 71 to 99 of VAP-C exhibits no homology to VAP-A and VAP-B, due to the frameshift. VAP-A and VAP-B form homo- or heterodimers via their TM domains, which is required for HCV replication (9, 44). To examine whether VAP-C is capable of interacting with VAP-A and VAP-B, FLAG-tagged VAP-A, -B, or -C was coexpressed with EE-tagged VAP-A or -B in 293T cells and was immunoprecipitated with the anti-FLAG antibody. Although EE-tagged VAP-A and VAP-B were coprecipitated with FLAG-tagged VAP-B and VAP-A, as reported previously, FLAG–VAP-C was precipitated with neither EE–VAP-A nor EE–VAP-B (Fig. 1B). These results indicate that VAP-C does not interact with VAP-A and VAP-B.

VAP-C binds to NS5B and interrupts the interaction of VAP-A and VAP-B with NS5B. VAP-A and VAP-B were identified as NS5A-binding proteins by yeast two-hybrid screening (9, 44). The coiled-coil domains of VAP-A and VAP-B were involved in the binding to NS5A, contributing to the efficiency of HCV replication (9, 44). However, VAP-C does not have the coiled-coil domain (Fig. 1A) and, therefore, VAP-C was expected not to interact with NS5A. To examine whether or not interaction between VAP-C and NS5A actually occurred, HA-tagged NS5A was coexpressed with FLAG-tagged VAP-A, -B, or -C in 293T cells and was immunoprecipitated with anti-HA antibody (Fig. 2). The results showed that the expression level of FLAG–VAP-C in the transfected cells was comparable to that of FLAG–VAP-A or FLAG–VAP-B (Fig. 2A, left). Although FLAG-tagged VAP-A and VAP-B were coprecipitated with HA-NS5A, no precipitation of FLAG–VAP-C with NS5A was detected (Fig. 2A, right), indicating that VAP-C does not interact with NS5A.

The RNA-dependent RNA polymerase NS5B was shown to interact with VAP-A through the MSP domain (44). The region spanning residues 1 to 70 of VAP-C is the same as the N-terminal-half region of the MSP domain of VAP-B and exhibits 77% homology to that of VAP-A (Fig. 1A). To exam-

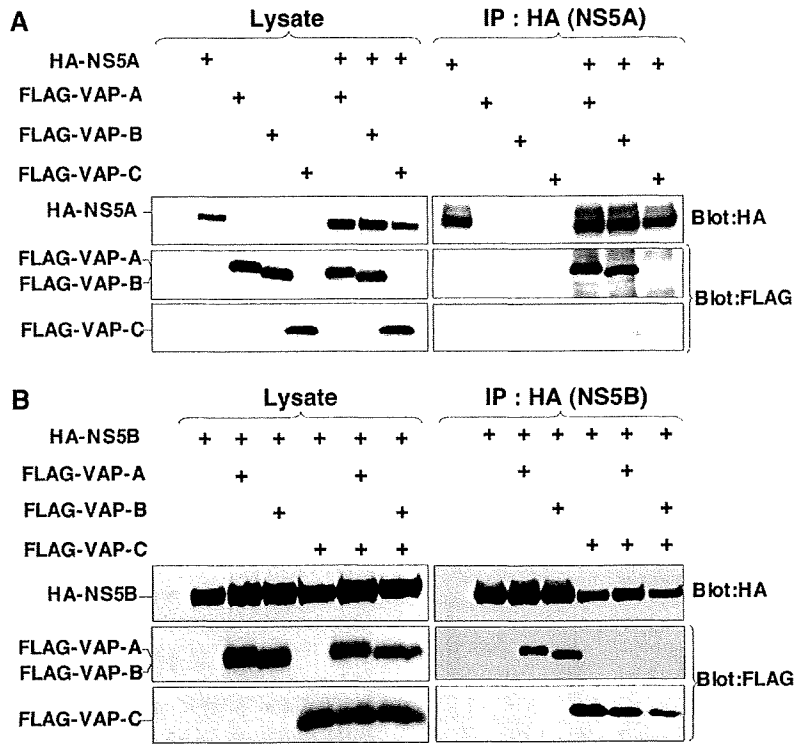

FIG. 2. VAP-C binds to NS5B but not NS5A and interrupts the interaction of VAP-A and VAP-B with NS5B. (A) The expression plasmids encoding NS5A or VAP proteins (1 μg each) were transfected into 293T cells after adjusting the total amounts of DNA to 2.0 μg with empty plasmid. HA-tagged NS5A was coexpressed with either FLAG-tagged VAP-A, VAP-B, or VAP-C in 293T cells and immunoprecipitated (IP) with anti-HA antibody, and the resulting precipitates were immunoblotted using anti-FLAG or anti-HA antibody. (B) The expression plasmids encoding NS5B or VAP proteins (1 μg each) were transfected into 293T cells after adjusting the total amounts of DNA to 3.0 μg with empty plasmid. HA-tagged NS5B was coexpressed with either FLAG-tagged VAP-A or VAP-B in the presence or absence of FLAG-tagged VAP-C in 293T cells and immunoprecipitated (IP) with anti-HA antibody, and the resulting precipitates were immunoblotted using anti-FLAG or anti-HA antibody. One percent of the lysate was used as an input control. The data in each panel are representative of the results of three independent experiments. +, present.

ine whether VAP-C is capable of interacting with NS5B, as are VAP-A and VAP-B, HA-NS5B was coexpressed with FLAG–VAP-A, FLAG–VAP-B, or FLAG–VAP-C in 293T cells and was immunoprecipitated with anti-HA antibody (Fig. 2B). Although substantial amounts of FLAG-tagged VAP-A, VAP-B, and VAP-C were coexpressed, and although all three were coprecipitated with HA-NS5B at comparable levels, the interaction of HA-NS5B with FLAG-tagged VAP-A or VAP-B was impaired by the coexpression of VAP-C, while FLAG–VAP-C was coprecipitated with HA-NS5B instead of FLAG-tagged VAP-A or VAP-B. These results suggest that VAP-C is capable of binding to NS5B and that the expression of VAP-C interrupts the interactions of NS5B with VAP-A and VAP-B.

Expression of VAP-C impairs the replication of HCV. VAP-A and VAP-B are known to support the replication of HCV RNA (2, 7). To examine the effect of VAP-C on the replication of HCV, FLAG–VAP-C was expressed in HCV replicon cells, Huh 9-13, in which a subgenomic HCV RNA of the genotype 1b strain Con1 was autonomously replicating. Huh 9-13 cells transfected with a plasmid encoding FLAG–VAP-C were harvested periodically up to 72 h posttransfection. The levels of replication of viral RNA and expression of NS5A were determined by real-time PCR and immunoblotting, respectively (Fig. 3). The expression of VAP-C reduced the intracellular RNA of the subgenomic HCV replicon in accordance with the incubation period after transfection with the expression plasmid of FLAG–VAP-C; the empty plasmid did not reduce the intracellular RNA (Fig. 3A). The expression of NS5A was gradually decreased and was undetectable at 72 h posttransfection, in contrast to the increase of VAP-C expression (Fig. 3B).

Next, to determine the effects of VAP-C expression on the replication of HCV, Huh 9-13 cells were transfected with 0 to 4 μg of the expression plasmid encoding VAP-A, VAP-B, or VAP-C and the replication of the subgenomic HCV RNA was determined at 48 h posttransfection. Although the HCV replicon cells transfected with 4 μg of a plasmid encoding FLAG–VAP-B exhibited enhancement of the RNA replication, those transfected with an equivalent amount of plasmid encoding FLAG–VAP-A or empty vector showed a slight reduction of HCV RNA replication. In contrast, the replicon cells transfected with a plasmid encoding FLAG–VAP-C exhibited a clear reduction of the HCV RNA replication in a dose-dependent manner (Fig. 3C). The expression of FLAG-tagged VAP-A, VAP-B, or VAP-C in the replicon cells was increased in correspondence with the amount of the transfected plasmid

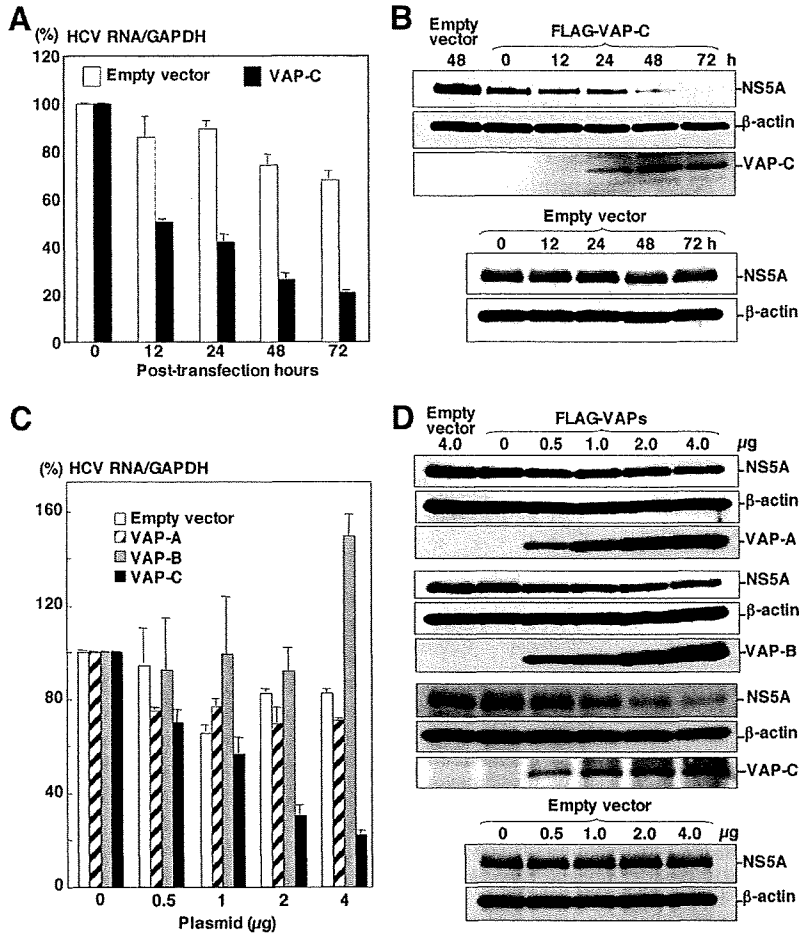

FIG. 3. Expression of VAP-C impairs the replication of HCV. (A) HCV replicon cells (Huh 9-13) were transfected with 4 μg of the expression plasmids encoding FLAG-tagged VAP-C or empty vector, and the level of intracellular HCV RNA was determined at 0, 12, 24, 48, or 72 h posttransfection by real-time PCR after normalization with GAPDH mRNA. The value of HCV RNA at 0 h posttransfection in the cell line transfected with the empty plasmid is represented as 100%. Data in this panel are shown as means ± standard deviations. (B) Huh 9-13 cells were transfected with 4 μg of the plasmid encoding FLAG-tagged VAP-C or empty plasmid, and the levels of expression of NS5A, β-actin, and VAP-C were determined at 0, 12, 24, 48, or 72 h posttransfection by immunoblotting using anti-NS5A, anti-β-actin, or anti-FLAG tag antibody. (C) Huh 9-13 cells were transfected with 0 to 4 μg of the plasmids encoding FLAG-tagged VAP-A, VAP-B, or VAP-C or empty vector, and the level of intracellular HCV RNA was determined at 72 h posttransfection as described for panel A. Data in this panel are shown as means ± standard deviations. (D) Huh 9-13 cells treated as described for panel C were harvested at 72 h posttransfection, and the levels of expression of NS5A, β-actin, VAP-A, VAP-B, and VAP-C were determined by immunoblotting. The data in each panel are representative of the results of three independent experiments.

(Fig. 3D), and the expression of NS5A was suppressed in accordance with the expression of FLAG–VAP-C, whereas the expression of FLAG–VAP-A and FLAG–VAP-B exhibited no effect on the expression of NS5A. These results suggest that the expression of VAP-C impairs the replication of HCV RNA.

VAP-C exhibits no effect on the IRES-dependent translation. The expression of VAP-C was shown to suppress the replication of the HCV RNA replication of the replicon cells. Next, to determine the effect of VAPs on the translation of HCV RNA, the reporter plasmid encoding the *Renilla* luciferase gene under the control of the CMV promoter and the firefly luciferase gene under the IRES of HCV, PV, or EMCV, in that order, was prepared as shown in Fig. 4. These reporter plasmids were introduced into Huh7OK1 cells 24 h after transfection of the expression plasmids encoding VAP-A, VAP-B, or VAP-C and harvested at 48 h posttransfection, and then the RLUs were determined. Although VAP-C exhibited a slight increase in the IRES-dependent translations of the HCV strains Con1 and JFH1, no significant effect of the expression of the VAPs on the HCV IRES-dependent translation was observed (Fig. 4A). Similarly, the expression of each of the VAPs in Huh7OK1 cells exhibited no significant effect on the IRES-dependent translation of PV or EMCV (Fig. 4B). These results indicate that the suppression of HCV RNA replication by the expression of

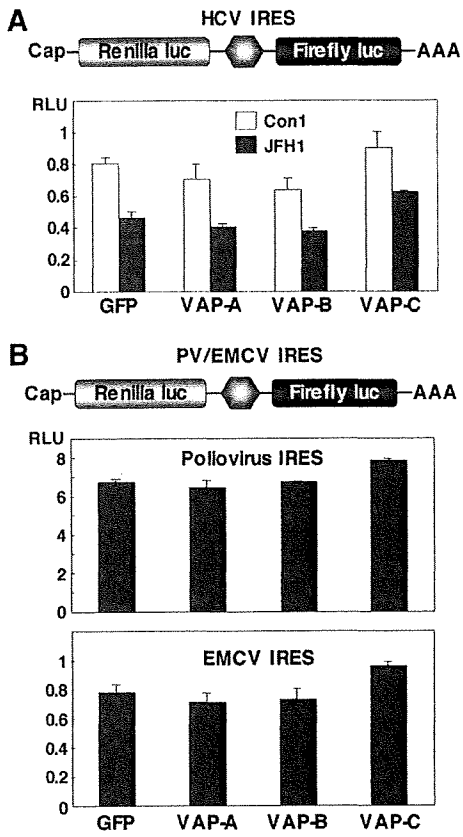

FIG. 4. VAP-C exhibits no effect on the viral IRES-dependent translation. (A) Top: structure of a reporter plasmid encoding the *Renilla* luciferase gene under the control of the CMV promoter and the firefly luciferase gene under the HCV IRES, in order. Bottom: the reporter plasmid was introduced into Huh7OK1 cells 24 h after transfection of the expression plasmids encoding VAP-A, VAP-B, or VAP-C, the cells harvested at 48 h posttransfection, and the RLUs determined after standardization with the expression of *Renilla* luciferase. (B) Top: structure of a reporter plasmid encoding the *Renilla* luciferase gene under the control of the CMV promoter and the firefly luciferase gene under the PV or EMCV IRES, in order. Bottom: each of the reporter plasmids was introduced into Huh7OK1 cells, and the RLU values were determined as described for panel A. Data in this figure are shown as the means ± standard deviations.

VAP-C was not due to the suppression of the IRES-dependent translation of the viral RNA genome.

VAP-C impairs HCV propagation. To examine the effect of VAP expression on HCV propagation, Huh7OK1 cells transfected with the expression plasmids encoding VAP-A, VAP-B, or VAP-C were infected with JFH1 virus, and the levels of production of the viral RNA, core protein, and infectious particles were determined at 96 h postinfection. The production of intracellular and extracellular viral RNA was increased up to 10 to 30 times and 2 to 3 times, respectively, by the expression of VAP-A or VAP-B whereas it was clearly decreased in a dose-dependent manner by the expression of VAP-C (Fig. 5A). Although the extracellular core protein was increased from 0.6 to 2.6 nmol/liter by the expression of VAP-A or VAP-B, as seen in the production of viral RNA, the intracellular core protein showed only a marginal increase (40 to 65 nmol/liter) (Fig. 5A). Although the reason for the discrepancy between the intracellular production of viral RNA and core protein is not known at the moment, some mechanisms other than RNA translation might be involved, because VAP expression exhibited no effect on the HCV IRES-dependent translation, as shown in Fig. 4A. In contrast to the enhancement of core protein production by the expression of VAP-A or VAP-B, the expression of VAP-C significantly reduced both the intracellular and extracellular expression of the core protein (Fig. 5A). Furthermore, the production of infectious particles in the culture supernatants of Huh7OK1 cells infected with JFH1 virus was slightly enhanced by the expression of VAP-A or VAP-B, whereas it was suppressed by the expression of VAP-C (Fig. 5A). To further confirm the effects of VAPs on the expression of HCV proteins, Huh7OK1 cells transfected with various amounts of the expression plasmids of VAP-A, VAP-B, or VAP-C and infected with the JFH1 virus were examined by immunoblotting (Fig. 5B). Although the expression of VAP-A or VAP-B exhibited no effect on NS5A expression, VAP-C expression clearly decreased the expression of NS5A in a dose-dependent manner. These results clearly indicate that the expression of VAP-C negatively regulates HCV propagation. Overexpression of VAP-C did not affect the endogenous expression of VAP-A or VAP-B (Fig. 5C), suggesting that suppression of HCV propagation by VAP-C is not due to the reduction of VAP-A or VAP-B expression.

Lack of VAP-C expression in human livers. VAP-C consists of the first 70 amino acid residues of VAP-B and the subtype-specific 29 amino acid residues derived from frameshift (Fig. 1A). The VAP-C-specific antibody generated by immunization with the peptide corresponding to the residues from 86 to 98 clearly detected VAP-C but neither VAP-A nor VAP-B in cells transfected with expression plasmids encoding FLAG-tagged VAP-A, VAP-B, or VAP-C (Fig. 6A). To determine the distribution of VAPs in human organs, the pool lysates of various organs prepared from several people were examined by immunoblotting (Fig. 6B). Expression of VAP-A was detected clearly in the kidney, lung, prostate, and liver; slightly in the duodenum, uterus, vagina, and bladder; and barely in the small intestine and stomach. VAP-B was detected clearly in the bladder, kidney, and prostate and slightly in the duodenum, small intestine, uterus, vagina, and liver. Expression of VAP-C was detected clearly in the stomach, uterus, kidney, and bladder; slightly in the duodenum, small intestine, and prostate; and barely detected in the vagina, lung, and liver. Several bands smaller than the expected size of VAP-C were observed in the stomach, duodenum, small intestine, uterus, vagina, prostate, and bladder. Because the main target of HCV replication is thought to be the liver, we next examined the expression of VAPs in individual human liver samples. VAP-A and VAP-B were clearly detected in the liver tissues obtained from chronic hepatitis C patients and a healthy donor, but no expression of VAP-C was detected (Fig. 6C). These results suggest that the expression of VAP-C may participate in the determination of tissue tropism of HCV propagation.

Substitution of Ser for Pro^{56} in VAPs leads to suppression of HCV replication. A single mutation of Pro^{56} to Ser (P56S) of VAP-B has been reported to be highly associated with amyotrophic lateral sclerosis (ALS), and the P56S mutation of VAP-B but not of VAP-A has been shown to induce large